NORTHWESTERN UNIVERSITY

ENHANCEMENT OF THE FRACTURE PROPERTIES OF THE BONE/CEMENT INTERFACE IN TOTAL JOINT REPLACEMENT

A THESIS

SUBMITTED TO THE GRADUATE SCHOOL

IN PARTIAL FULFILLMENT OF THE REQUIREMENTS

for the degree

MASTER OF SCIENCE

Field of Theoretical and Applied Mechanics

By

John William Steege

Evanston, Illinois

June 1987

There is a correlation of -0.98 between the annual birthrate in Great Britain, from 1875 to 1920, and the annual production of pig iron in the United States.

Yule, G. U., 1920[1]

1 Yule, G. U., J. Royal Statist. Soc., 89:1, 1926.

Abstract

Fatigue data is generated for bimaterial (bone/polymethylmethacrylate) four-point bending test specimens. Conceptualization of crack growth data is achieved as a series of stable growth periods interrupted by discrete occurrences of cement posts characterized by zero crack growth. Results of previous finite element models of the test specimen with and without a cohesive zone present at the bone/polymethylmethacrylate interface are employed in determining the cyclic stress intensity factor (ΔK) at the crack tip.

Multi-variate statistical analysis is performed on the data in an attempt to: 1) relate crack propagation rate ($\Delta a/\Delta N$) to ΔK, PMMA penetration depth, and bone strength for the stable crack growth periods; and 2) relate the same factors to the number ($Post_N$) and duration (ΔN_{post}) of zero crack growth periods. A final predictive equation is obtained along with statistical significance levels for the modeled crack growth behavior. It is generally found that crack growth is retarded for increasing cement penetration, bone strength, and $Post_N$ while the inclusion of a cohesive zone plays little role in the final results.

It is then proposed to enhance the interface by the introduction of artificial posts. The final predictive equation is optimized for $Post_N$ on the dichotomy that as $Post_N$ is increased, the bone strength decreases and thus $\Delta a/\Delta N$ increases, yet $\Delta a/\Delta N$ decreases as the number of posts increases. Based upon the optimized results and several biomechanical considerations, a 'crack arrestor' device is designed for and tested qualitatively in the four-point bending test specimen. Results are encouraging and recommendations are made for further development and study of the 'crack arrestor' concept.

Committee Members

Jack L. Lewis (Chairman)

Leon M. Keer

Lyle F. Mockros

Acknowledgments

It has been a sincere honor to have been associated with the Northwestern Rehabilitation Engineering Program during my years as a part time graduate student. The friends, colleagues, and mentors I have encountered during this period have contributed more to this thesis and my life than they will ever realize. I am forever appreciative of them.

I am especially grateful to Jack Lewis, who plucked me from the waning days of undergraduate life to guide and shape my professional and academic career as a bio-mechanical engineer immeasurably. Also of great help in the creation of the devices used in this work was the gifted John Schmidt. My friends Terry Nicola and J.P. Clech deserve special recognition as the pioneers of this unique approach to the study of the bone/cement interface. Karen Hanmer was of great help in the creation of many of the figures of this work. Lastly, I am indebted to Northwestern University for allowing me the opportunity and financial benefits to obtain this degree over my years as a full time employee. I sincerely wish for this policy to continue so that others may benefit as I did.

I would like to dedicate this work to my wife, Victoria, and my parents, Robert and Barbara, whose constant encouragement throughout my life as a graduate student made it all possible.

Table of Contents

List of Tables

List of Figures

Chapter Four

Appendix A

CHAPTER ONE

INTRODUCTION

1.1 Statement of the Problem

A widely used and highly successful surgical procedure for the treatment of patients with severe arthritis and other joint disorders is total joint replacement. It has been estimated that thirty million Americans are afflicted with arthritis [74] while four million of these people are severely disabled [75]. Approximately 200,000 patients are treated each year in the United States with total joint replacement. Although the vast majority of these procedures provide immediate and drastic relief from pain and disability, many (depending upon the involved joint) will not have a clinically acceptable result [26]. In addition, these procedures are seldom used in the younger, more active patient due to concern of failure.

Loosening of prosthetic joint components secured to bone with PMMA (polymethyl-methacrylate) bone-cement remains the most common problem with these devices. There are current attempts being made to perfect bony ingrowth fixation techniques, but it is likely that even with its shortcomings, cement fixation will remain the method of choice for the forseeable future.

Fixation of joint replacement components to bone by polymethylmethacrylate bone-cement is achieved by a mechanical interlock of the cement into porous, trabecular cancellous bone. Pressures developed by insertion of components have been found to be insufficient to achieve adequate penetration in many cases [73]. In order to maximize the penetration of the cement, techniques have been developed to prepare the surface and to apply the cement to the bone under pressure. Various authors have reported on the use of pressurization systems including cement compactors [50], cement guns [29], and hydro-static compressed gas supplies [16]. 'Water Lavage' systems whose purpose is to remove

fat and marrow from bone interstices allowing greater cement penetration have been tested and are in use [41,44]. The main advantage of these techniques is that they increase the depth of cement penetration into bone [3,4,16,17,29,37,47,50,51,68], and thus, theoretically, the bone/cement interface strength. Also, a technique that 'precoats' bone with an initial layer of cement which is then subjected to a second cement layer has been reported [32].

The first mechanical tests performed on the interface were simple tensile and shear tests [3,4,17,28,29,31,68]. These experiments generally found that mechanical strength did indeed increase with increasing penetration and pressurization. However, bone area-fraction and bone strength have also been mentioned as important factors influencing interface strength [3,31,51,68], while the time duration of cement pressurization has not been conclusively shown to effect the interfacial strength [3,51,68].

Researchers, noting that increased usage of PMMA can lead to increased thermal damage (bone necrosis) during the acrylic's exothermic reaction [8,12,63], increased release of excess toxic monomer into the blood stream [9,18], and increased PMMA debris found in the operated joint [18], have suggested optimal cement penetration depths based on these tensile and shear tests. These recommended values range from 3 to 4 mm [3,68].

However, even with penetration depths at or near these levels, loosening of total joint components may continue. It has been postulated that the appearance of a radiolucent line (Figure 1.1) at the bone/cement interface in radiographs of total joint implants is an indication of loosening [39,53]. It has been reported in clinical studies of total hips that 19, 24, 47, and 55 percent show some degree of radiolucency at mean follow-up times of 3, 5, 3, and 3 years respectively [66,7,25,60]. Even more striking are follow-up reports of total knee replacements where 18, 36, and 96 percent developed some radiolucency after 4, 5, and 2.5 years respectively [20,67,27]. The Northwestern University Rehabilitation

Engineering Program's own in house study of the Kinematic™ Knee indicates that these radiolucent lines preferentially develop at lower penetrations, but with time will develop even when the depth of cement penetration is at the 'optimal level' [76].

Often, a thin fibrous tissue is found at the location of the radiolucency, and is thought to be the radiolucency on x-ray [8,12,21,49,52,67,69]. This tissue has been associated with and has been considered a precursor to component idiopathic loosening. Debate continues as to why this fibrous liner forms. Some investigators have proposed that its formation is the result of a biological reaction to load environment and/or implant material [18,21,49,52,63]. Alternatively, it has been suggested that the tissue growth follows mechanical failure of the interface [12,69]. This mechanical failure could be viewed as crack growth through the bone, the cement, the bone/cement interface, or any combination of these. It is this second postulate, that component loosening is due to mechanical failure of the bone/cement interface, that will be examined in this thesis.

The purpose of this work was to determine if a previously proposed [13,45] four-point bending mechanical model of failure at the bone/cement interface was capable of quantifying the fatigue behavior of the interface and if so, whether it could be used to improve the strength of the interface.

This required reducing previous data [45] and performing further four-point bending fracture tests to develop a statistical model of the interface which would define crack propagation not only as a function of the cyclic stress intensity factor ΔK, but also as a function of bone quality and depth of cement penetration. In addition, the effect of inclusion of a cohesive zone (as determined by Clech) on the statistical model was sought. Finally, several tests using the four-point bent beam fatigue protocol were run with proposed mechanical improvements for the bone/cement interface which were based upon the empirical model of crack propagation at the interface.

1.2 Mechanical Failure of the Interface: Review of Previous Work

1.2.1 Bone

Several researchers have examined the fracture properties of bone. Most of the studies have involved push-out tests on bovine bone. Fracture mechanics measurements on both three-point bending and compact tension specimen tests have been performed on compact bone. Mean critical stress intensity factors (K_c) of 3.2, 3.6 and 4.0 $MPam^{1/2}$ have been reported respectively [6,38,71]. Few studies have been performed on human cancellous bone due to limitations on specimen size. Moyle and Bowden [43] found that, as in the bovine studies, the work of fracture for human femoral bone increased with bone density. There are few, if any, reports of normal *in vivo* human bone fracturing in fatigue although Alman and Frasca [1] reported the relative ease with which some diseased bones fracture. Certainly stress fractures occur in bone, but it has been hypothesized that the cement lines surrounding osteons act as crack arrestors [11], perhaps explaining the absence of catastrophic fatigue fracture of bone. This, coupled with the possibility that the bone (if not necrotic) may actively be repairing itself casts doubt on the importance of bone fracture in the mechanics of the interface. A summary of various bone fracture and fatigue studies is given in Table Ia.

1.2.2 Polymethylmethacrylate

Perhaps the most highly scrutinized component of the interface is the bone-cement (polymethylmethacrylate). Failure and breakage of the cement has been documented *in vivo* [60,67]. Documentation of crack initiation, initial flaw size, or cement micro-cracking is scarce. It has been demonstrated (Figures 1.2-1.4) that crack initiation, in some cases, may occur around cement voids or around cement inclusions [65]. It could be that

the cracks noted are the result of mechanical release of residual cement stresses which have been shown to occur [10]. It has yet to be shown, however, that these crack initiators lead to the *in vivo* cement failure and breakage noted above.

Crack growth was proposed early as a mechanism for cement failure [5,22,62]. Subsequently, much work was done comparing the critical stress intensity factors and energy release rates for various clinical cements, experimental cements, and cement preparation and application techniques [55,58,64,72]. Others have made similar comparisons using cement fatigue strength or fatigue life as their criteria [19,23,30,64]. Some have attempted to compare *in vivo* cement bulk strains to cement fatigue life [48], but the relevance of cement bulk strains to interface strains is unclear. The load rates used by these investigators ranged from 2 to 23 Hz. while fatigue testing cements in fully reversed tension-compression cycles [19,23,30,48,64,72]. O'Conner et al., however, found a significant increase in cement fatigue life when tested at 2 Hz. as compared to 20 Hz. [48]. A summary of various cement fatigue and fracture studies is given in Table Ib.

1.2.3 Bone/Cement Interface

The most likely region of fracture failure is at the interface itself. Some work has been done in this area and is the chief topic of this thesis. Mak [35,36] tested compact tension specimens composed of fixed bone and Simplex-P bone-cement and found rough relationships between PMMA interdigitation and the critical stress intensity factor. He concluded that if a tensile stress of 1 MPa is present at the edge of a tibial component (a stress predicted by Askew, et al.[2]), flaws as small as 1-2 mm could initiate cracks in poor (low cement penetration) interfaces. Flaws of this size can commonly be seen in clinical radiographs as shown in Figure 1.5. Mak's study used single cycle tests and generally involved low cement penetration values.

Further investigation by Lewis et al. [33,34] concluded that possibly no cement/bone interface would be completely resistant to fatigue. Nicola [45] performed four-point bending fracture fatigue tests and used Shaw's [61] finite element results for his specimen configuration to determine the applied cyclic stress intensity factor. He frequently noted formation of a secondary crack through cement after a primary crack had propagated through the entire bone/cement interface. Propagation of this second crack would lead to catastrophic failure. Other phenomena of note were formation of a crack in compression regions, micromotion between cement and bone ahead of the crack tip, and fluid flow between cement and bone. A rough relationship was found between the cyclic stress intensity factor and the crack propagation rate. Similarly, Ryd has documented varying degrees of micromotion at the interface by using Roentgen Stereophotogrammetric Analysis [59].

Clech et al. have developed mathematical models for the 2 crack case [14] and the compressive crack situation [15]. Both models employ a cohesive zone along a portion of the propagating crack. Clech [13], modeling the cohesive zone as a set of linear springs whose stiffness was obtained experimentally, used a version of Shaw's comparative finite element technique to determine the stress intensity factor in relation to crack length with and without a cohesive zone for the four-point bending test configuration used in this study and described in Chapter Two. It was found that inclusion of a cohesive zone slightly reduced the stress intensity factor at the crack tip and that the magnitude of this reduction increased with increasing cohesive zone length.

CHAPTER TWO

METHODS AND PROCEDURES

Fresh cancellous bone was taken from several distal femora and proximal tibiae obtained from amputation or autopsy and which had been stored frozen at -22° Celsius. Bone was cut into cubic specimens 25 x 15 x 12.5 mm in dimension on a low speed rotary Buehler Isomet thin sectioning saw (Buehler, LTD., Lake Bluff, IL) using a diamond impregnated blade and water as a cutting fluid. All bone specimens were taken from within 1 cm from the joint's articulating surface. In general, the 12.5 mm dimension was oriented parallel to the long axis of the donor bone (the z-axis in Figure 2.1). From the remaining bone most proximal to the joint, 5 x 5 x 5 mm bone cubes were cut on the Isomet saw (for compressive bone strength tests described later) which corresponded to the 25 x 15 mm surface of the previously described bone specimens. All bone was then stored frozen at -22° Celsius until it was fashioned into four-point bending specimens or compressively tested.

To form the four-point bending specimens, bone cubes were placed at the bottom of the jig shown schematically in Figure 2.2 such that the 25 x 15 mm surface which had been proximal to the articulating knee joint was face up. The L-shaped walls of the jig were clamped together with two C-clamps. To preform an initial crack, a thin razor blade was placed into the groove of the jig so it lay over approximately 15 x 5 mm of the stronger edge of the 25 x 15 mm bone surface (as determined by the compression testing of bone described later). From micrometer measurements, the razor's thickness was found to be 100 μm with a correspondingly smaller radius of curvature at the tip, thus allowing for a very thin initial crack . A slender piece of elastic rubber with initial width slightly larger than the groove opening was stretched until it fit snugly into the groove and over the razor blade. The elastic was then released from tension so as to clamp the razor

edge firmly over the bone surface. A visual check was made to confirm that the elastic edge did not overlap the razor's edge and any necessary adjustments made.

Eight to ten grams of Simplex-P Bone-Cement (Howmedica Inc., Rutherford, NJ) was mixed in the usual ratio of monomer to powder (1 ml : 2 gm) and stirred at 2 Hz. for 30 seconds. After 90 seconds the cement was poured through a long plastic funnel until it completely covered the top of the bone surface at a thickness of approximately 10 mm. An aluminum block the size of the shaft of the jig and attached to the end of a rod was slipped into the shaft and lowered until it rested on top of the cement. After 120 seconds the bone- cement had begun to reach the doughy stage. At this point, the assembly was placed on the ram of a MTS materials testing machine (model 810, MTS Inc., Minneapolis, MN). At 135 seconds from the beginning of the cement mix, the piston (rod and block) was loaded under load control to either 12.9 Newtons (6 specimens) or 51.7 Newtons (10 specimens) for 5 seconds. These loads created pressures in the cement of 34 KPa (5 psi) and 138 KPa (20 psi) respectively. The assembly was removed from the ram and the cement allowed to set for 30 minutes. Specimens were then removed from the jig and stored frozen at -22° Celsius. Note that one specimen was pressurized by hand at an unknown low load.

After formation of the interface, zero magnification x-rays of the specimen were taken to determine depth of penetration of the cement into the bone (Figures 2.3 and 2.4). The approximately 20 mm interface was divided into four equal zones. Using a micrometer, the maximum depth of penetration for each zone was determined and the mean for the entire interface calculated. The radiographs of the specimens were also examined by three independent observers and their degree of penetration graded on a scale of one to three, with one being low and three being high. Good agreement was found between the measured values and the observer grades.

For the final stage of specimen preparation, the frozen sample was thawed to room temperature and its remaining bone surface (i.e. the surface not interdigitated with bone-cement), was gnarled by use of a long steel pin. This surface was then subjected to an air jet which acted to remove fat and tissue from the interstices of the bone. The initial crack opening was filled with Parafilm (American Can Co., Greenwich, CT) and the entire specimen wrapped in several layers of Parafilm. The sample was clamped into the jig shown schematically in Figure 2.5. Aluminum bars, each weighing 70 grams, were slid into each end of the jig and a small gap left between the tip of each bar and the surfaces of the specimen. Several grams of Zimmer Low Viscosity Cement powder (Zimmer Inc., Warsaw, IN) and Truweld Acrylic monomer (D. L. Saslow and Co., Chicago, IL) were prepared and poured into these gaps. The bars were pushed further inwards and clamped into place. The cement was allowed to cure for 30 minutes and the test piece, now in the form of a beam, was placed into a refrigerator at 5° Celsius to await testing the following day.

The de-fatting of the support interface was done to preferentially strengthen that interface in the fatigue tests. Also, the tips of the aluminum bars were grooved in a grid-like fashion to allow interlock of the cement with the metal. This interface will henceforth be refered to as the metal support interface. The beam specimen was thawed to room temperature and to assist in visual monitoring of crack growth, a small scale (millimeter) was attached onto the PMMA adjacent to the approximately 20 mm long visible interface, using Thermoplastic Cement (Buehler LTD., Lake Bluff, IL). Also, for most of the specimens, a one inch gage length extensometer (model 632.11B-20, MTS Systems Corp., Minneapolis, MN) was affixed across the initial crack mouth by use of elastic bands and was used to measure crack mouth opening. Placement of the gage relative to the crack mouth was recorded. This assembly was placed in a four-point bending jig which was suspended between the 1000 pound load cell and ram of the materials testing

machine (Figures 2.6 and 2.7). Thus load was measured either as a function of ram stroke or crack mouth opening on an X-Y plotter.

Load was applied linearly from no load to full bending and then linearly relieved. Specimens were loaded at between 1.00 and 1.67 Hz. A relatively low frequency was chosen because it was feared that load rate might effect crack propagation through the cement spicules due to plasticity effects at the crack tip. Also a factor in the choice of a low load rate was the proximity of a 1 Hz. loading rate to ambulation. If a step length of 2/3 meters is assumed, a walking speed of 2.4 km/hr (1.5 mph) is simulated at a rate of 1 Hz.

1 cyc/sec x 0.5 strides/cyc x 1.3 m/stride x .001 km/m x 3600 sec/hr = 2.4 km/hr {2.1}

Primary and secondary crack growth was measured visually through a Bausch and Lomb Stereozoom triocular microscope (model 1070P, Rochester, NY). Measurements were usually made at 13x magnification and were facilitated by a 100 division vernier in one of the eyepieces and the attached millimeter scale mentioned previously. At each recording of crack length, the number of cycles was documented and the X-Y plotter was activated yielding a load vs crack mouth opening curve. Data was recorded on a regular basis, but no attempt was made to gather it during exact cycle intervals. The triocular scope allowed for photographic, motion picture, and video documentation of specimens.

Definition of the crack tip was difficult but was accomplished by adhering to the following criteria. For the primary crack, the tip was defined as the point on the interface where motion between the bone-cement and bone originated. The tip of the secondary crack was defined as the point where separation between the cement and bone edges was approximately 125 μm. This width was selected after observation of various specimens.

Specimens were loaded each working day to maximum loads ranging from 35 to 489 Newtons. If the initial crack were ignored and simple beam theory employed, these

loads would create approximate maximum tensile stresses of between 0.2 to 3 MPa, which are in the range of values predicted by some finite element analyses of total joint implants. Due to the lack of complete automation, testing would be halted at the end of each day. The specimen would then be soaked in saline, sealed in plastic wrap, and stored at 5° Celsius until the next working day. This procedure was not the most desirable, but since the crack lengths appeared the same at the start of a new day, it was felt to be satisfactory. Cyclic loading continued in this fashion until approximately 500,000 cycles had been reached or until catastrophic failure of the interface.

The cross-sectional area (perpendicular to the long axis of the donor bone) of the previously cut 5 x 5 x 5 mm bone cubes was measured with a micrometer. The cubes were compressively loaded to failure in the direction of the long axis of the donor bone at a displacement rate of 0.4 mm/min on the MTS. The compressive strength of each cube was calculated from the failure load and the measured cross-sectional area of each cube. An average compressive strength of the 12 cubes which corresponded to the interfacial region was determined for each specimen. Bone strength values were also classified into three grades where: 1 was < 3 MPa, 3 was > 6 MPa, and 2 was in between.

Data was manipulated and analyzed using The Statistical Package for the Social Sciences [46] statistics programs.

CHAPTER THREE

RESULTS

In all, 26 specimens were prepared and tested. To allow for more cases, results of 10 specimens tested by Nicola [45] which were felt to fit the specifications of this study were employed. Of all the specimens, 8 were of tibial stock while 18 were of femoral stock. Raw descriptive data for all test specimens is presented in Table II.

In accordance with the results of Nicola [45], two cracks were seen at the interface. The first crack, henceforth refered to as the primary crack (a_p), was the leading crack and would form between the bone and cement. The other crack, henceforth refered to as the secondary crack (a_s), would follow the primary crack and grow through a combination of cement, bone, and interface. This secondary crack can be thought of as the end of the cohesive zone modeled by Clech [14]. A typical interface with both crack types is pictured in Figure 3.1. Due to the dynamic nature of the primary crack, only the secondary crack may readily be documented on still photographs. Motion picture and video documentation of the cracks exists for demonstration purposes.

3.1 Definition Of Terms

α : crack extension exponent

a_p : primary crack length (mm)

a_s : secondary crack length (mm)

Ar^2 : variance adjusted by : $\frac{r^2 - (\#\text{ variables} - 1)}{(\#\text{ cases} - \#\text{ variables})} \times (1 - r^2)$

β : bone strength grade exponent

BSG : grade of the bone strength (1, 2, 3) as defined earlier

C_i : regression constants

Δa : crack extension in millimeters

$\Delta a/\Delta N$: crack propagation rate in millimeters per cycle

ΔN_i : number of cycles

ΔN_{post} : number of cycles to pass through a given post

i : subscripts 1-4 associated with defined regions

κ : stress intensity factor exponent

ΔK : cyclic stress intensity factor in $MPam^{1/2}$

NS : not statistically significant at the 0.05 level

ρ : cement penetration depth exponent

λ : cohesive zone length in millimeters $(a_p - a_s)$

PEN : penetration of cement in millimeters

$Post_N$: # of discontinuities (posts) along an interface

p_{sig} : statistical significance level based on F value

r : multiple correlation coefficient

r^2 : square of r (variance in dependent variable explained by the independent variables in a linear relationship)

3.2 General Observations

3.2.1 Strength of the Interface

If an interface possessed a reasonable amount of cement penetration and was of average bone quality, it would exhibit some resistance to interface fracture. The typical crack mouth opening was of the order of 120 μm as measured by the extensometer during stable crack growth and the maximum measured, just preceding catastrophic failure, was 800 μm. A typical maximum crack opening as measured by Clech when determining the linear region of the cohesive zone was 320 μm. This implies that typically, in these fracture tests, the cement spicules are not pulling out of the cancellous bone but rather are failing through fatigue. Typical plots of load vs crack opening and crack opening vs cycles are presented in Figures 3.2 and 3.3 respectively. Table II presents initial crack opening data.

To determine the amount of initial crack opening due to interface separation, a three-dimensional finite element model (8 noded linear isoparametric brick elements) of the beam specimen was created and analyzed using SAP IV™ [77]. Material values used in the model are reported in Table IV and a crack length of 5 mm was given to the model by setting material values of elements at the crack site to those of air. A load of 178 Newtons was applied to the model to appropriately simulate the experimental four-point bending situation. The loaded model is presented in Figure 3.4.

Nodes were identified on the model which corresponded to the attachment points of the extensometer. The finite element analysis calculated displacement between these points in the crack opening direction was 55 μm. For the actual specimens which were loaded to 178 Newtons, the mean bone strength was 5.8 MPa, the mean initial crack length was 4.9 mm, and the mean initial displacement was 49 μm.

Therefore, the crack opening from the finite element model (perfectly connected mesh

in pure bending) is virtually indistinguishable from the experimental results, implying that the initial interface between the bone and cement is very well connected. The fact that the opening grows as a function of cyclic load is a testimony to the interfaces susceptibility to fatigue crack growth.

This fatigue of the cement spicules, which range in size from 150 to 300 μm in diameter, can be seen on light and scanning electron microscopy photographs of a specimen (Figures 3.5-3.7). However, regardless of an interface's strength and its eventual failure through the cohesive zone (i.e. propagation of the secondary crack), it should be remembered that the primary loosening crack propagates ahead of and relatively faster than the secondary crack and may provide a means of soft tissue generation.

3.2.2 Permanent Crack Opening

A phenomenon noted in this study which may also facilitate the formation of soft tissue at the interface was the permanent deformation of the interface after cyclic loading (Figure 3.8). This phenomenon was further demonstrated by observing the output of the extensometer attached across the crack mouth. After each cycle, the zero point of the gage would increase slightly, indicating that the cement and the bone had separated slightly (see Figure 3.2). Optical measurement of the attachment points of the gage assured that the extensometer was not slipping relative to the interface. Perhaps this deformation is due to plasticity of the cement, damage to the bone, slip of the cement spicules relative to bone, rupture of the cohesive zone, or a combination of all these factors. It should be noted that this separation occurred at a nearly linear constant rate as measured by the gage.

3.2.3 Random Penetration At Constant Pressure

As noted in other studies [3,68], it was found that cement penetration is not solely dependent upon applied pressure and bone strength and may vary widely from case to case

as shown in Table II. For instance, specimens S1b and S6b have equal cement application pressures and bone strengths yet their resulting average penetration depths are 2.48 and 5.30 mm respectively. This inability to consistently achieve a uniform cement layer (and thus cohesive zone) is one implant parameter that could be improved to create a superior interface.

3.3 Analysis

Equations were statistically formed from the data to predict the total number of cycles needed to achieve a given crack extension (or crack mouth opening) as a function of bone strength (density), cement penetration, and the computed cyclic stress intensity factor at the crack tip.

3.3.1 Relation of Crack Mouth Opening to Crack Length

The relationship between crack mouth opening as measured by the extensometer to the primary crack, secondary crack, and cohesive zone length was plotted in Figure 3.9. In general, by using linear regression, the crack mouth opening was found to significantly increase with a_p ($r^2 = 0.50$) and a_s ($r^2 = 0.69$) but not with λ. Subsequent attempts to more highly correlate the two variables via multivariate analyses which included the effects of bone strength, cement penetration depth, and extensometer gage placement did not prove fruitful. No further attempts were made to correlate λ with the analytical model.

3.3.2 Initial Analysis of Crack Growth

The cyclic stress intensity factor (ΔK) was determined for both a_p and a_s using the results of Clech. Its value was determined for each crack length with and without the effects of a cohesive zone. The exact calculations for determining ΔK are reported in

Appendix A. In general, Clech used a comparative finite element technique between two crack problems with identical meshes at the crack tips. One problem's analytical solution for the stress intensity factor is known while the second, in this case the bimaterial no-slip four-point bent beam configuration, is unknown. Clech shows that the ratio of the two problems' crack opening displacements obtained from the finite element analysis is equal to their ratios of stress intensity factors.

Attention will be directed at the primary crack with the assumption that the secondary crack simply defines a cohesive zone which forms behind the primary crack. Plots of primary crack length versus cycle were generated for each specimen and typically were of the form of Figure 3.10. In general, the crack propagation rate varied widely with stress level and cement penetration level as depicted in Figures 3.11 and 3.12. Δa and ΔN were determined from the plots for each specimen across all of the combined regions two and three. Multiple regression analysis was performed across regions 2 and 3 using this data. Multiple regression is a general statistical technique through which it is possible to analyze the relationship between a dependent or criterion variable ($\Delta a/\Delta N$) and a set of independent or predictor variables (PEN,BSG,ΔK). The main focus of the technique is the evaluation and measurement of overall dependence of a variable upon a set of other variables.

For each multiple regression analysis subsequently reported, variable transformations were performed to allow for linear-linear, linear-log, log-linear, and log-log analyses. Without exception, the log-log (or power law) regressions provided the most highly correlated results. Similarly, regression was performed with both ordinal and categorical values of penetration and bone strength with best results being obtained for ordinal values of penetration (PEN) and categorical values of bone strength (BSG). For clarity, these are the only statistical results reported. It should be noted also that the power law format is the standard format of fracture mechanics equations.

The results of the regression were:

$$\Delta N = C \times \frac{PEN^{\rho} \times BSG^{\beta}}{\Delta K^{\kappa}} \times \Delta a \qquad \{3.1\}$$

Computed Values

Variable	Value	p_{sig}
C	0.4070	0.64 (NS)
β	3.1400	0.009
ρ	2.9095	0.002
κ	2.4218	0.005
r^2	0.59	
Ar^2	0.51	0.001

3.3.3 A Hypothesis to Better Model Crack Growth

From observations of the general behavior of propagating cracks, a hypothesis was developed as to how they could more accurately be described compared to the results of the preceding section 3.3.2. The behavior of a_p in the four-point bending tests was divided into four regions as depicted in Figure 3.10. These regions were then defined as follows:

1. The primary crack has just begun and it is free of any cohesive forces. This is a relatively short lived effect where the crack extension (Δa) is small, the cohesive zone length (λ) is small or nonexistent, and the number of cycles (ΔN) is low.

2.1 As the crack length extends past region 1, the cohesive zone comes into existence. The presence of cohesive forces in this zone reduces the stress applied at the crack tip from what it would be without a cohesive zone as demonstrated by Clech [13]. In general, this region of growth is quite linear and constant.

3. There appear discontinuities in the propagation of the crack which are defined as region 3. These are hypothesized as occurring due to the crack tip encountering a large PMMA post(s). The crack then requires a given number of cycles, ΔN_{post}, to propagate through or around the post. The magnitude of ΔN_{post} will depend upon the mean post size and its stress environment. The mean post

size can be considered a function of cement penetration level and the specimen's bone density or strength.

Also, multiple discontinuities may occur in each specimen, thus the number of region 3's encountered or alternatively the post density ($Post_N$) may possibly be described by crack length, cement penetration level, and bone strength.

Alternatively, the discontinuities may be due to the crack tip propagating near to the neutral axis of the beam and into a low stress field while the bulk of tensile stresses is absorbed by the cohesive zone, halting crack growth until further failure of the cohesive zone. For this situation to occur, the length of the cohesive zone would initially be larger than half the length of the initial interface or approximately 10 mm. As shown in Table III, the mean cohesive zone size was less than this value (4.15 mm). To forgo this alternate scenario from occurring, data obtained after the primary crack had propagated past the initial neutral axis was rejected. It should be noted here that this alternate mode of discontinuity occurrence could be valid *in vivo* .

2.2 Crack propagation is occurring via the same mode as in 2.1 after a discontinuity has been overcome. Similarly, as mentioned above, additional discontinuities may be encountered.

4. Failure through the cohesive zone has and is occurring, and in a good number of cases is continuing through the bone. This region is primarily the result of quick and catastrophic propagation of the secondary crack.

By breaking the behavior of the crack into the regions described, it was thought that descriptive equations for each region could more completely describe the propagation of the primary crack. In general:

$$\text{Cycles to failure} = (\text{cycles region 1}) + (\text{cycles region 2}) + (\text{cycles region 3}) + (\text{cycles region 4}) \quad \{3.2\}$$

Using linear regression analysis, equations of crack length as a function of cycle were obtained for regions 1, 2, and 4 of each specimen. Except for region 4, the correlation coefficients and the significance levels were high ($r > 0.9$, $p_{sig} < 0.05$) for each region of every specimen. With these equations, values of $\Delta a/\Delta N$ were calculated for each region of

every specimen. The $\Delta a/\Delta N$ values were then compiled into separate data files for each region along with associated bone strength, penetration, and average ΔK values. The occurrences of discontinuities were also identified from these plots and the duration in cycles, bone strength, penetration, and ΔK values associated with each occurrence were recorded and stored in a separate data file. Multiple regression analyses were performed on each data file to provide descriptive equations of crack growth in each generalized region.

Region 1 was studied and a descriptive equation is reported in section 3.3.6, but in general, the number of cycles in region 1 was small. Likewise the number of cycles in region 4 was small while the propagation rate was nonlinear and the propagation mode irregular. Therefore, regression results for region 4 are not reported. Thus the total number of cycles was generalized as:

$$\Delta N_{tot} = \Delta N_2 + \Sigma[\Delta N_3] \qquad \{3.3\}$$

Summarizing the hypothesis for regions 2 & 3 in equation form and keeping in mind that the crack growth rate is a function of ΔK, bone strength, and penetration:

region 2: $\Delta N_2 = (\Delta N_2 / \Delta a) \times \Delta a \dashrightarrow \Delta N_2 / \Delta a\{\Delta K, BSG, PEN\} \times \Delta a$ {3.4}

region 3: $\Sigma[\Delta N_3] = Post_N \times \Delta N_{post}$

$\dashrightarrow Post_N\{\Delta a, BSG, PEN\} \times \Delta N_{post}\{\Delta K, BSG, PEN\}$ {3.5}

Several points should be kept in mind while considering regression results reported in the following sections:

1. Effects of compression cracks such as those reported by Nicola and modeled by Clech have not been taken into account.

2. For the data in cohesive crack region(s) 2, the cyclic stress intensity factor is calculated from the average crack length in that region. Thus, if in this region

the crack grew from 8 to 10 mm, Δa would be 2 mm and the crack length used to find the stress intensity factor from Clech's result would be 9 mm.

3. With the possible alternative cause of crack propagation discontinuities in mind, a discontinuity occurrence (region 3) was only considered valid if:
   a) controlled crack propagation continued after the occurrence; and
   b) in general, the crack length at the time of the occurrence was less than half of the total interface length.

4. The calculation of the cyclic stress intensity factor is based upon the assumption that there is no slip at the interface. This is most likely the case for moderate penetration interfaces, but may not be the case for low penetration interfaces. In fact, in one low penetration case, a definite but slight shear displacement was noted between the bone and the cement mass. Therefore, the stress intensity values reported for low penetration cases may be a small source of error in any subsequent analysis.

3.3.4 Regression Equation For Regions 2

$$\Delta N_2 = C_2 \times \frac{BSG^{\beta} \times PEN^{\rho}}{\Delta K^{\kappa}} \times \Delta a \qquad \{3.6\}$$

Computed Values

Variable	Value	p_{sig}
C_2	0.80204	0.03
β	2.2717	0.03
ρ	3.2314	0.001
κ	2.2166	0.001
r^2	0.60	
Ar^2	0.56	0.001

If the material parameter values of penetration and bone strength were omitted from the analysis, the computed values became:

Variable	Value	p_{sig}
C_2	4.8×10^{18}	0.001
$\beta = \rho$	0.0	
κ	20.8	0.15 (NS)
r^2	0.03	
Ar^2	0.03	0.15 (NS)

Thus it can be seen that inclusion of the variables PEN and BSG substantially aids in the description of the behavior of the primary crack for region 2.

3.3.5 Regression Equations For Region(s) 3

3.3.5.1 *Number of Discontinuities*

$$Post_N = C \times \frac{\Delta a^{\alpha} \times PEN^{\rho}}{BSG^{\beta}} \qquad \{3.7\}$$

Note: At zero crack growth, the value $Post_N$ was assumed to be zero for regression purposes.

Computed Values

Variable	Value	p_{sig}
C	0.28046	0.01
β	0.39923	0.416 (NS)
ρ	0.31910	0.411 (NS)
α	0.81747	0.001
r^2	0.98	
Ar^2	0.98	0.001

If the material parameter values of penetration and bone strength were omitted from the analysis, the computed values became:

Variable	Value	p_{sig}
C	0.30562	0.001
$\beta = \rho$	0.0	
α	0.81775	0.001
$r^2 = Ar^2$	0.98	0.001

Thus the inclusion of material parameters BSG and PEN yielded no more accurate

results than their omission. Therefore, their effect on the number of posts encountered will be ignored henceforth.

3.3.5.2 *Number Of Cycles To Pass Through A Post*

$$\Delta N_{post} = C \times \frac{PEN^{\rho} \times BSG^{\beta}}{\Delta K^{\kappa}} \qquad \{3.8\}$$

Computed Values

Variable	Value	p_{sig}
C	7.56225	0.21 (NS)
β	3.02865	0.025
ρ	1.94555	0.10 (NS)
κ	2.00579	0.004
r^2	0.45	
Ar^2	0.39	0.002

If the material parameter values of penetration and bone strength were omitted from the analysis, the computed values became:

Variable	Value	p_{sig}
C	1.29×10^3	0.001
$\beta = \rho$	0.0	
κ	0.37041	0.14 (NS)
r^2	0.08	
Ar^2	0.04	0.14 (NS)

Thus it can be seen that inclusion of the variables PEN and BSG substantially aids in the description of the behavior of the primary crack for region 3.

3.3.6 Regression Equation For Region 1

$$\Delta N_1 = C_1 \times \frac{BSG^{\beta} \times PEN^{\rho}}{\Delta K^{\kappa}} \times \Delta a \qquad \{3.9\}$$

(see equation 3.6)

Computed Values		
Variable	Value	p_{sig}
C_1	0.0227	0.004
β	2.3506	0.04
ρ	2.4453	0.02
κ	2.3319	0.02
r^2	0.69	
Ar^2	0.57	0.02

If the material parameter values of penetration and bone strength were omitted from the analysis, the square of the multiple correlation factor became:

$$r^2 = Ar^2 = 0.001$$

Therefore this result was considered meaningless and equation {3.9} accepted as valid.

3.3.7 Development Of A Final Equation

Combining equations {3.3} and {3.5} yields:

$$\Delta N_{tot} = \Delta N_2 + [Post_N \times \Delta N_{post}] \qquad \{3.10\}$$

Therefore, insertion of computed values for equations {3.6, 3.7, and 3.8} into equation {3.10} yields:

$$\Delta N_{tot} = \Delta a \times 0.80204 \times \frac{BSG^{2.2717} \times PEN^{3.2314}}{\Delta K^{2.2166}} + 7.5623 \times \frac{\Delta a^{0.81775} \times PEN^{1.9455}}{BSG^{3.0287} \times \Delta K^{2.0058}} \qquad \{3.11\}$$

Which describes crack growth for regions 2 and 3. In approximate terms (in mm/cycles):

$$\frac{\Delta a}{\Delta N_{tot}} = \frac{BSG^3 \times \Delta K^2}{PEN^2} \times \frac{1.25}{(PEN \times BSG^5 + 9.5)} \qquad \{3.12\}$$

3.4 Examination of the Cohesive Zone

The preceding analysis incorporated ΔK's calculated as if no cohesive zone existed. Analysis was performed using Clech's results for a 4 mm cohesive zone at the interface, however there was no significant difference between those results and the results reported in section 3.3. There may be several reasons for this:

1. The actual length of the cohesive zone (λ) varies from specimen to specimen and from crack length to crack length. It may extend the length of the interface or may be very small. It can be seen from Figure 3.10 that λ was unrelated to the primary or secondary crack ($r^2 < 0.39$) and varied widely throughout the tests. From Table III it is seen that the mean cohesive zone length for these tests was approximately 4 mm with a standard deviation of 2 mm. Clech, in his analysis, used a typical cohesive zone length which varied with the crack length from 1 to 5 mm (Figure 3.13). The inability in this work to use the actual cohesive zone length data for each individual specimen in the calculation of ΔK may have led to the insignificance of the cohesive zone model to the results.

2. Clech found that the cohesive zone played little beneficial role to the interface at short crack lengths and only really became effective at longer crack lengths (i.e. ΔK decreased by 19% for $a_p/w = 0.7$ and $\lambda = 4$ mm). In this study, however, at longer crack lengths the cohesive zone had either inevitably decreased in length and catastrophic failure of the interface had begun (region 4) or become so large as to allow the crack tip to approach the neutral axis and thus disqualify the data as discussed in section 3.3.3.

3.5 SUMMARY

1. Increasing penetration dramatically increases the resistance to crack propagation rate (Figure 3.11 and 3.12). In fact it can be seen from equation {3.12} that the effect of cement penetration is greater (cubic) than that of the applied stress field (squared). This may indicate that with appropriate penetration, mechanical interface failure may be delayed.

2. The effect of bone strength or bone density on the integrity of the interface is less apparent. This lack of clarity may be due in part to an 'optimum value' relation between bone strength and the tensile interface strength as described by Askew et al. [3]. Namely, as bone strength increases (allowing for a stronger interface), bone void size decreases accounting for less volume of penetrated cement. This points out that as there is an optimum penetration depth, there exists an optimum bone density for implant fixation. Attempts to model the bone quality in this manner in the statistical analyses did not yield more statistically significant results.

3. The prediction equation {3.11} is based on limited material parameter value ranges as reported in Table II. Therefore an interface possessing material parameter values outside these ranges, specifically cement penetration depth, may not correspond to the reported results. There may be decreasing benefits of increasing cement penetration into bone over the optimal penetration level mentioned previously.

4. To determine the accuracy of the predictive equation {3.11} in forcasting crack growth with respect to actual data, a descriptive parameter similar to multiple r^2 was developed. The parameter, which will be called Nr^2, was of the form:

$$Nr^2 = 1 - \frac{\Sigma (x_i - \chi_i)^2}{\Sigma (x_i - X)^2} \qquad \{3.13\}$$

where:

x_i is the experimental value of ΔN for each case (i)

χ_i is the predicted ΔN from equation {3.11} based on the experimental values of Δa, ΔK, PEN, and BSG for each case (i)

X is the experimental mean of all ΔN

It is generally accepted that the square of the correlation coefficient represents the percentage of the variance of the phenomenon (ΔN) being explained by the multiple regression analysis. Similarly, Nr^2 represents the percentage of variation of ΔN which is explained by the descriptive equation {3.11}. Using the data of $\Delta a/\Delta N$ collected for section 3.3.2, the Nr^2 obtained was 0.60 and the adjusted Nr^2 (computed like Ar^2 was computed in section 3.1) was 0.52.

Note the similarity of equations {3.11} and {3.1}. Note also that equation {3.1} possesses almost the same relative adjusted variance as equation {3.11} (Ar^2 & Nr^2 : 0.51 & 0.52). Thus the hypothesized modeling of posts at the interface provides no better (or worse) explanation of the interfacial fracture mechanics than the elementary multiple regression analysis reported in section 3.3.2. However, the coefficient of equation {3.1} is highly insignificant and in fact has a large standard error when compared to those of equation {3.11}. Although 50 to 60 percent of behavior has been explained and the significance level on almost all of the exponents is meaningful, when the actual data is plotted along with the predictive equations (Figures 3.14-3.17), it can be seen that the scatter is large and thus the model should only be considered a rough guide to interface crack behavior.

There could be several reasons why the hypothesized model is unable to explain crack growth at a higher level. There may exist independent variables other than those measured affecting crack behavior. Secondly, there may be some inherent error in the measurement of the independent variables. For instance, the cement penetration measured via radiography is based upon a two-dimensional image as opposed to the actual three-dimensional cement/bone interlock situation. Similarly, the bone area-fraction as opposed to the compressive bone strength may be the optimal parameter to describe the interface. Possibly of great aid in the improvement of the method would be the creation of a family of curves of $\Delta K/\sigma$ vs a_p /w for varying cohesive zone lengths as opposed to the one set presented by Clech and used in this study (see Figure A.1). Overall, there seems to be some (as yet undefined) interaction between the cement penetration and the cancellous bone microstructure which would probably be of greater significance in the description of crack propagation at the interface.

Perhaps most importantly, the relatively low number of samples (there were 26 total specimens) contributes greatly to the lack of a higher correlation. The introduction of the hypothesized post model allowed for 36 measurements of region 2 and 25 measurements of region 3. If it is assumed that the three independent variables ΔK, PEN, and BSG may be defined by three categories each or 27 combinations overall, and as a general statistics rule that five measurements are required for each combination, it may then be postulated that 135 measurements are needed to assure statistical soundness. As can be seen from these tests, the number of measurements for the hypothesized post model is approximately equal to the number of specimens. Therefore, 135 specimens would need to be tested in order to provide a completely sound statistical

conclusion. In addition, certain cells of the 27 proposed may be difficult to physically obtain (i.e. low PEN, low BSG, and high ΔK) and therefore may necessitate an even larger number of specimens to be created and tested before a successful test is conducted. The testing of such a large sample size is beyond the scope of this thesis.

The necessity of such a large sample size to test proposed interface improvements (such as lavage of bone or vacuum mixing of cement) makes use of this test protocol as an evaluation method of the bone/cement interface difficult. Certainly testing would have to be performed on a large scale, perhaps involving several loading apparatus. Additionally, the rate of loading may be increased, but the effects of a higher rate on results are unclear. Of great help would be automation of crack growth monitoring. Unfortunately, standard crack measurement systems, such as foil gages or extensometers, are not directly suitable to the biological bimaterial interface involved.

Lastly, it was felt that even with its shortcomings, the hypothetical post model provided a good qualitative understanding and a sufficiently accurate quantitative description of the interface to allow for its use in the following chapter in an attempt to improve the bone/cement interface.

CHAPTER FOUR

DESIGN OF AN IMPROVED BONE/CEMENT INTERFACE

4.1 Optimize Equation {3.11} For $Post_N$

4.1.1 Reasoning

It is now proposed to introduce relatively large metal posts into the bone/cement interface aside from the normal cement spicules present. It can indirectly be seen from equations {3.10} and {3.12} that the number of posts present has an optimal value in relation to the crack propagation rate. To see this it must be understood that for a constant cement post size, an increase in the number of posts will lead to a decrease in the area-fraction of bone present. A decrease in bone area-fraction gives rise to a decrease in bone strength, thus in equation {3.12}, an artificial increase in $Post_N$ will lead to a decrease in BSG and thus a slight increase in the crack propagation rate. Note from equation {3.10} however, that the same increase in $Post_N$ gives rise to a decrease in the crack propagation rate by increasing the total number of cycles. Therefore there must be an optimal artificial post density for an interface which is dependent upon existing bone strength and cement penetration.

4.1.2 Assumptions And Equations

An expression for a bone's new area-fraction as a function of the number of artificial posts introduced into the interface must be formulated. Therefore:

$$AF_{new} = \frac{AF \times AREA - AP \times Post_N}{AREA} \qquad \{4.1\}$$

where AF represents bone area-fraction, AP represents the area of a post and AREA is the total specimen surface area.

Now assume initially a post diameter of 3 mm. Therefore:

$$AP = \pi \times (0.0015)^2 = 7.069 \times 10^{-6} \ [m^2]$$

and the total bone surface area used in these tests is:

$$AREA = 0.02 \times 0.015 = 3.0 \times 10^{-4} \ [m^2]$$

Therefore:

$$AF_{new} = \frac{(AF \times 0.0003) - 7.1 \times 10^{-6} \times Post_N}{0.0003}$$

$$AF_{new} = AF - (0.0736 \times Post_N) \qquad \{4.2\}$$

Since $Post_N$ will vary with the bone strength, the design process will have to be specific to a given bone strength. For tibial bone, from the results of Goldstein [24]:

$$BS = 0.0265 \times E \text{ (Young's modulus of bone)} \qquad \{4.3\}$$

and for the medial edge, E = 336 MPa so BS = 8.90 MPa

and for the central area, E = 54 MPa so BS = 1.43 MPa

Relating bone compressive strength to area-fraction with the results of Williams and Lewis [70]:

$$BS_{yield} \, [MPa] = 0.246 + 23.0 \times AF \qquad \{4.4\}$$

Substituting a form of equation {4.4} into equation {4.2} and the result back into equation {4.4} yields:

$$BS_{new} = BS_{old} - (0.5419 \text{ x } Post_N) \qquad \{4.5\}$$

To combine this equation with the final statistical equation {3.11}, BS must first be related to BSG. Using linear regression and assuming that if:

$$BSG = 1, \text{ that } BS = 1.5 \text{ MPa}$$

$$BSG = 2, \text{ that } BS = 4.5 \text{ MPa}$$

$$BSG = 3, \text{ that } BS = 7.5 \text{ MPa}$$

Therefore:

$$BSG = 0.5 + 0.333 \text{ x } BS[MPa] \qquad \{4.6\}$$

Combining equations {4.5} and {4.6} yields:

$$BSG_{new} = 0.5 + 0.333 \text{ x } BS_{old} - 0.1806 \text{ x } Post_N \qquad \{4.7\}$$

Combining equations {3.6, 3.7, 3.10, and 4.7} yields the total number of cycles ΔN for a crack to progress a given length Δa as a function of BS_{old}, ΔK, PEN, and finally $Post_N$. The resulting equation is:

$$\{4.8\}$$

$$\Delta N_{tot} = \frac{0.80204 \text{ x } \Delta a \text{ x } PEN^{3.2314} \text{ x } \left(0.5 + \frac{BS_{old}}{3} - 0.1806 \text{ x } Post_N\right)^{2.2717}}{\Delta K^{2.2166}}$$

$$+ Post_N \text{ x } \frac{7.5623 \text{ x } PEN^{1.9456} \text{ x } \left(0.5 + \frac{BS_{old}}{3} - 0.1806 \text{ x } Post_N\right)^{3.0281}}{\Delta K^{2.0058}}$$

If typical values are chosen for the first three variables, equation {4.8} may be optimized as a function of $Post_N$. A simple optimization program was written and variable conditions chosen.

For values of: $\Delta K = 0.5\ MPam^{1/2}$ (A relatively high value)

$PEN = 1.5$ mm

$\Delta a = 20$ mm (length of interface); and

$BS_{old} = 8.90$ MPa [from Goldstein et al.; 24]

The value for penetration in equation {4.8} will be held constant throughout the design process at 1.5 mm which is one half the proposed length (3 mm) of the artificial posts and is based upon the previously mentioned results of Askew et al. and Walker et al. [3,68]. It is chosen as an approximation of the average depth of cement penetration across the interface.

For a bone compressive strength of 8.9 MPa, an optimal $Post_N$ of 3.7 for every 20 mm of interface was found. If an initial bone strength of 1.43 MPa was assumed, $Post_N$ optimal became negative and in fact only became positive for initial bone strengths greater than 2.55 MPa.

These results are based upon and are dependent upon all of the previous assumptions and chosen constants. For instance, fewer posts would be needed at lower stress levels and higher average penetration. Alternatively, if a smaller post diameter was chosen, more posts would be needed.

The result that weaker bone should require fewer posts seems intuitively incorrect. However, for a post to be effective, it must have viable bone to interact with. This result indicates that for weak bone, a strong interface is unattainable due to its dependence upon bone strength. It is therefore more advantageous to retain the healthy bone (although weak) rather than alter the stress field with posts.

4.2 Design of a Test Specimen Crack Arrestor

4.2.1 General Configuration

It can be seen from the preceding section 4.1.2 that the number of artificial posts desired at an interface may range from none to a very high concentration and is dependent upon several factors. $Post_N$ ranged (as a function of bone density) from 0 to 4 along the 20 mm interface. Clinically, 2.6 MPa is fairly weak bone while 8.9 MPa is very dense cancellous bone. Thus, to implement the results, $Post_N$ was chosen to be 2 along the linear 20 mm interface in order to approximate average bone quality.

The insertion of 2 posts into the 20 x 15 mm surface of the bone specimen could be accomplished by placing one set of two posts down the center of the specimen, two ridges across the width of the specimen, or by addition of multiple sets of posts across the width of the specimen. To preserve as much bone as possible but provide as much stability to the interface as possible, the latter design configuration was chosen.

Because the interface along which the crack propagates is 20 mm in length, the distance between the center of the 3 mm diameter posts was chosen to be 10 mm. Since the bone specimen is 15 mm wide, it was possible to place two sets of posts into the specimen. The proposed design is shown in Figure 4.1. It may be seen that the post length of 3 mm has been employed. The posts have been bored (1 mm) to facilitate insertion and promote cement interlock. Also, a center vent hole has been added to the device to alleviate lateral flow of cement upon device insertion. Some of the characteristics of the device design are discussed below.

4.2.2 Thickness of the Plate

The amount of plate flexion and the radial stresses developed in the plate due to this bending should be considered. Analysis is presented in Appendix B. Considering a near

point load of 2000 Newtons (3 x body weight) between posts it is found that for a titanium plate thickness of 1 mm, the maximum deflection is 132 μm with a maximum radial stress of 2181 MPa, while for a thickness of 2 mm, the maximum deflection is 16.5 μm with a maximum radial stress of 545 MPa. Considering that 132 μm is of the order mentioned for typical crack mouth opening (120 μm), 2 mm was considered a more acceptable thickness.

4.2.3 Fillet At Post/Plate Junction

The junction between the plate and post should be rounded in order to reduce stress concentration at this point and to prevent eventual fatigue failure of a post. Employing a formula reported in [57] for a circular beam on a plate, it was found that for titanium, the fillet may be very small indeed ($r << 0.25$ mm). From a clinical standpoint, the smaller the fillet, the more flush the fit of the device with the bone surface and thus the less likely plate bending or stress shielding of bone will occur. Details of this analysis are presented in Appendix C.

4.3 Testing of the Device

4.3.1 Procedure

The device shown schematically in Figure 4.1 was manufactured from steel and is pictured in Figures 4.2-4.3. Fracture tests on bone employing the same methodology described in chapter two were performed with the following exceptions.

1. The metal device was grit blasted, passivated for 30 minutes in 30% V/V Nitric acid, and rinsed thoroughly in distilled water prior to specimen formation in accordance with ASTM standard F87.

2. Using a steel template (Figure 4.2), four holes were drilled into the bone to a depth of 3 mm using a hand drill. This was done to accept the artificial posts of the device. The diameter of the holes was made slightly larger (175 μm) than the 3 mm diameter of the posts.

3. PMMA was poured directly onto the bone surface and the device then slid into the holes in the bone by hand, thus pressurizing the cement. More PMMA was poured over the device and then gently pressurized by hand with the cement block and piston. Pressure on the PMMA was not generated by use of the MTS due to the need to assure that the device had become flush with the bone surface. This required the use of unknown moderate hand pressure. However, cement penetration and device/bone fit were documented by x-ray.

4.3.2 Results

Three initial fracture tests of the device were conducted. The raw data of these tests is reported in Table II. Of note in Table II is that none of the specimens failed, but rather were stopped for separate reasons. Specimen A5d was simply halted after 500,000 cycles and statically loaded to failure at 706.2 Newtons (158.8 lbs.) through a subinterface layer beneath the posts pictured in Figure 4.5. Specimen A6d (which was loaded at 311 N) behaved differently. At 20,200 cycles the cement-metal bond failed and the device pulled cleanly out of its cement mantle. It was then conjectured that the introduction of artificial metal posts may not be necessary, but rather the presence of large artificial cement posts may be sufficient to arrest crack growth. Therefore, specimen A6d was refabricated with Simplex-P cement replacing the device by repolymerizing with the existing cement mantle. Testing continued at 311 Newtons with the primary and secondary cracks appearing unchanged from before the cement-metal failure. Testing was halted at 83,000 due to imminent failure of the cement/bone support interface. Specimen AZ5a was stopped after 216,000 cycles and not taken to failure but behaved similarly to A5d.

Finite element analyses were performed as in section 3.2.1 with the inclusion of the metal device or simply PMMA posts. The initial crack openings predicted by the analyses were 46 and 56 μm respectively for a 178 Newton load and 5 mm initial crack. As can be seen from Table II, initial crack openings for the crack arrestor samples were below this value (even at higher loads) indicating very good initial fixation.

Crack opening and extension vs cycles is plotted in Figures 3.3 and 3.12 respectively for specimens A5d and A6d. It can be seen from these figures that the addition of the artificial posts reduced crack mouth opening and the crack growth rate. More impressive is the fact that specimen A6d possessed a poorly penetrated interface within a high stress environment.

The material parameter values and appropriate data for these specimens were then applied to equation {3.11} to obtain perspective on their superior performance. For A5d, a total number of 15,000 cycles was expected for the recorded crack extension while the actual number of cycles was at least 499,000. For A6d, a total number of 2,700 cycles was expected for the recorded crack extension while the actual number of cycles was at least 82,000 before the test was stopped. For AZ5a, a total number of 109,000 cycles was expected for the recorded crack extension while the actual number of cycles was 216,000 before the test was stopped.

CHAPTER FIVE

CONCLUSIONS

In general, it has been demonstrated that the crack propagation behavior of the bone/cement interface is a function of cement penetration, bone strength and the cyclic stress intensity factor at the crack tip. As mentioned in section 3.5, more tests are needed to statistically refine the relationships of the variables included in this study. A device was designed which did, on a qualitative basis, dramatically reduce crack propagation through the interface. It, too, requires further testing with the four-point bent beam protocol to conclusively define its beneficial effects.

Clinically, there are several more considerations to take into account before this device should actually be implanted. As mentioned previously, a real design concern is that stress shielding of the bone surface between posts may occur. If this were to happen, the underlying bone may resorb. Another consideration would be to make the posts of the arrestor of varying lengths to prevent a possible subinterface layer from forming which may in itself (especially in conjunction with surface bone resorption) be a source of failure.

This design was formulated as a separate component in an implant system. It remains to be shown whether the concept of crack arrestors would be better implemented by direct placement of the artificial posts on a tibial component. Intuitively this would simplify the implantation of the device although the subsequent loss of vent holes in the design may damage the integrity of the cement/device/bone mechanical interlock.

As in the case of specimen A6d, the interface may best be enhanced by providing artificial cement posts of various sizes and depths in the bone matrix in accordance with the optimization of equation {4.8}, a surgically obtainable objective. Alternatively if metal posts were to be used, cement precoating of the metal posts to prevent metal-cement separation may be advisable.

Also, for any implant scheme, a gradient of post density should be incorporated into the design to match varying tibial subchondral bone strengths as reported in the literature. In this preliminary design and testing of a crack arrestor device, a post density was chosen for moderate bone strength. Further testing should be done to verify the postulate that a lower post density should be employed in weaker bone. This probably cannot be shown in mechanical tests since for any post density failure will most often occur through the weaker bone. Animal models should alternatively be developed to show the value of saving weak bone not for mechanical purposes but rather for the general health of the interface.

REFERENCES

[1] Alman, B., Frasca, P., "Fracture Failure Mechanism in Patients with Osteogenesis Imperfecta", Trans. 31st O.R.S., Vol. 10, 1985, pg. 209.

[2] Askew, M.J., Lewis, J.L., Jaycox, D.P., "Comparative Evaluation of Total Knee Prosthesis Designs", Proc. Int. Conf. on Rehab. Eng., Toronto, June 1980.

[3] Askew, M.J., Steege, J.W., Lewis, J.L., Ranieri, R., Wixson, R.L., "Effect of Cement Pressure and Bone Strength on Polymethylmethacrylate Fixation", J. Orthopaedic Research, Vol. 1, 1984, pp. 412-420.

[4] Bean, D.J., Hollis, J.M., Woo, S.L-Y, Convery, F.R., "Sustained Pressurization Effects on the Bone/Cement Interface", Trans. 31st O.R.S., Vol. 10, 1985, pg. 146.

[5] Beaumont, P.W., Young, R.J., "Failure of Brittle Polymers by Slow Crack Growth", J. Mat. Sci., Vol. 10, 1975, pp. 1334-1342.

[6] Behri, J.C., Bonfield, W., "Fracture Mechanics of Bone – The Effect of Density, Specimen Thickness, and Crack Velocity on Longitudnal Fracture", J. Biomechanics, Vol. 17, 1984, pp. 25-34.

[7] Bekenbaugh, R.D., Ilstrup, D.M., "Total Hip Arthroplasty: A Review of Three Hundred and Thirty Three Cases With Long Follow-up", J. Bone Joint Surg., Vol. 60-A, 1978, pp. 306-313.

[8] Bloebaum, T.A., Gruen, T.A., Sarmiento, A., "Interface and Bone Response to Increased Penetration of Acrylic Cement", Trans. 10th Soc. for Biomaterials, 1984, pg. 82.

[9] Bloch, B., Haken, J.K., Hastings, G.W., "Evaluation of Cold Curing Acrylic Cement for Prosthesis Stabilization", Clinical Orthopaedics, Vol. 72, 1970, pp. 239-241.

[10] Burke, D.W., O'Conner, D.O., Harris, W.H., "Residual Acrylic Cement Stresses in Total Hip Arthroplasty", Trans. 32nd O.R.S., Vol. 11, 1986, pg. 286.

[11] Burr, D.B., Frederickson, R.G., Schaffler, M.B., "Does the Composition of the Cement Line Allow it to Act Effectively as a Crack Arrestor?", Trans. 31st O.R.S., Vol. 10, 1985, pg. 207.

[12] Charnley, J., "Acrylic Cement in Orthopaedic Surgery", Williams and Wilkins, Baltimore MD, 1970.

[13] Clech, J.P., "Fracture Mechanics of the Bone-Cement Interface in Total Joint Replacements", Ph.D dissertation, Northwestern University, Evanston IL, June 1985.

[14] Clech, J.P., Keer, L.M., Lewis, J.L., "A Crack Model of the Bone Cement Interface", J. Biomech. Eng., Vol. 106, 1984, pp. 235-243.

[15] Clech, J.P., Keer, L.M., Lewis, J.L., "A Model of Tension and Compression Cracks With Cohesive Zone at a Bone-Cement Interface", Submitted to J. Biomech. Eng., 1986.

[16] Convery, F.R., Malcom, L.L., "Prosthetic Fixation with Controlled Pressurized Polymerization of Polymethylmethacrylate", Trans. 26th O.R.S., Vol. 5, 1980, pg. 77.

[17] Cooke, F.W., Cipolletti, G.B., Lunceford, E.M., Sauer, B.W., "The Influence of Surgical Technique on the Strength of Cement Fixation", Trans. 24th O.R.S., Vol. 3, 1978, pg. 89.

[18] Crout, D.H., Corkill, J.A., James, M.L., Ling, R.S., "Methylmethacrylate Metabolism in Man", Clinical Orthopaedics, Vol. 141, 1979, pp. 90-95.

[19] Davies, J.P., O'Connor, D.O., Green, J.A., Harris, W.H., "A Comparison of the Tensile and Fatigue Strengths of Simplex-P, LVC, and Zimmer Regular Bone Cement", Trans. 31st O.R.S., Vol. 10, 1985, pg. 241.

[20] Ewald, F.C., Jacobs, M.A., Miegel, R.E., Walker, P.S., Poss, R., Sledge, C.B., "Kinematic Total Knee Replacement", J. Bone Joint Surg., Vol. 66-A, 1984, pp. 1302-1040.

[21] Freeman, M.A.R., Bradley, G.W., Revell, P.A., "Observations Upon the Interface Between Bone and Polymethylmethacrylate Cement", J. Bone Joint Surg., Vol. 64-B, 1982, pp. 489-493.

[22] Freitag, T.A., Cannon, S.L., "Fracture Characteristics of Acrylic Bone Cements: I. Fracture Toughness", J. Biomed. Mat. Res., Vol. 10, 1976, pp. 805-828.

[23] Gates, E.I., Carter, D.R., Harris, W.H., "Comparative Fatigue Behavior of Different Bone Cements ", Clinical Orthopaedics, Vol. 189, 1984, pp. 294-299.

[24] Goldstein, S.A., Wilson, D.L., Sonstergard, D.A., Mathews, L.S., "The Mechanical Properties of Human Tibial Trabecular Bone as a Function of Metaphyseal Location", J. Biomechanics, Vol. 16, 1983, pp. 965-969.

[25] Gruen, T.A., McNeice, G.M., Amstutz, H.C., " 'Modes of Failure' of Cemented Stem-Type Femoral Components", Clinical Orthopaedics, Vol. 141, 1979, pp. 17-27.

[26] Hori, R.Y., Lewis, J.L., Zimmerman, J.R., Compere, C.L., "The Number of Total Joint Replacements in the United States", Clinical Orthopaedics, Vol. 132, 1978, pp. 46-52.

[27] Insall, J.N., Lachiewicz, P.F., Burstein, A.H., "The Posterior Stabilized Condylar Prosthesis: A Modification of the Total Condylar Design", J. Bone Joint Surg., Vol. 64-A, 1982, pp. 1317-1323.

[28] Kolbel, R., Bergmann, G., Boenick, U., "Mechanical Properties of the Cement/Bone Bond", In: Engineering in Medicine 2, Eds. Schaldach and Hehmen, Springer-Verlog, N.Y., 1976, pp. 347-357.

[29] Krause, W.R., Krug, W., Miller, J., "Strength of the Cement-Bone Interface", Clinical Orthopaedics, Vol. 163, 1982, pp. 290-299.

[30] Krause, W.R., Mathis, R.S., "Fatigue Properties of Current Acrylic Bone Cements", Trans. 10th Soc. for Biomaterials, 1984, pg. 349.

[31] Kusleika, R., Stupp, S.I., "Mechanical Strength of Poly(methylmethacrylate) Cement-Human Bone Interfaces", Journal of Biomed. Mat. Res., Vol. 17, 1983, pp. 441-458.

[32] Lane, T., Pratt, G.W., Poss, R., Rosenthal, D., "PMMA Bone Precoating – A New Technique to Optimize the Bone-Cement Interface", Trans. 28th O.R.S., Vol. 7, 1982, pg. 247.

[33] Lewis, J.L., Nicola, T., Keer, L., "Mechanical Fatigue Failure of the Bone Cement Interface of Joint Implants", ASME Biomechanics Symposium, 1983, pp. 35-38.

[34] Lewis, J.L., Nicola, T., Keer, L.M., Clech, J.P., Steege, J.W., Wixson, R.L., "Failure Processes at the Cancellous Bone-PMMA Interface", Trans. 31st O.R.S., Vol. 10, 1985, pg. 144.

[35] Mak, A.F., "Fracture Mechanics of the PMMA-Cancellous Bone Interface", Ph.D. dissertation, Northwestern University, Evanston IL, June 1980.

[36] Mak, A.F., Lewis, J.L., "Fracture Mechanics of the PMMA/Cancellous Bone Interface", 1980 ASME Advances in Bioengineering, 1980, pp. 209-212.

[37] Markolf, K.L., Amstutz, H.C., "Penetration and Flow of Acrylic Bone Cement", Clinical Orthopaedics, Vol. 121, 1976, pp. 99-102.

[38] Melvin, J.W., Evans, F.G., "Crack Propagation in Bone", ASME Biomaterials Symposium, Detroit, MI, 1973.

[39] Mendes, D.M., "Roentgenographic Evaluation in Total Hip Replacement. A Study of 100 McKee-Farrar Prosthetic Replacements", Clinical Orthopaedics, Vol. 95, 1973, pp. 104-110.

[40] Meyers, P.R., Lautenschlager, E.P., Moore, B.K., "On the Setting Properties of Bone Cement", J. Bone Joint Surg., Vol. 55-A, 1973, pg. 149.

[41] Miller, J.E., Burke, D.L., Krause, W., Kelebay, L.C., "An Experimental Technique for Improved Fixation of Implant Components in Human Total Knee Arthroplasty", Trans. 25th O.R.S., Vol. 4, 1979, pg. 303.

[42] Miller, J., Burke, D.L., Stachiewicz, J.W., Kelebay, L., "A Study of the Interface Between Polymethylmethacrylate and Living Cortical Bone Under Conditions of Load Bearing", Trans. 22nd O.R.S., Vol. 1, 1976, pg. 191.

[43] Moyle, D.D., Bowden, W., "Fracture of Human Femoral Bone", J. Biomechanics, Vol. 17, 1984, pp. 203-213.

[44] Narten, N.C., Clarke, D., Greenwald, A.S., Wilde, A.H., "An Effective Technique for Bond Enhancement at the Bone-Cement Interface", Trans. 24th O.R.S., Vol. 4, 1978, pg. 64.

[45] Nicola, T.L., "Failure of the Cancellous Bone-Cement Interface in Total Knee Joint Replacements", M.S. dissertation, Northwestern University, Evanston IL, 1984.

[46] Nie, N., Hull, C.H., Jenkins, J.G., Steinbrenner, K., Bent, D.H., "SPSS; Statistical Package for the Social Sciences."

[47] Noble, P.C., Swarts, E., "The Penetration of Acrylic Bone Cement Into Cancellous Bone", Proc. of the 5th Annual Conf. on Rehab. Eng., 1984.

[48] O'Connor, D.O., Burke, D.W., Davies, J.P., Harris, W.H., "S-N Curve for Centrifuged and Uncentrifuged PMMA", Trans. 31st O.R.S., Vol. 10, 1985, pg. 325.

[49] O'Connor, J., Goodfellow, J.W., Perry, N., "Fixation of the Tibial Component of the Oxford Knee", Orthop. Clin. North Am., Vol. 13, 1982, pp. 65-87.

[50] Oh, I., Bourne, R.B., Harris, W.H., "The Femoral Cement Compactor: An Improvement in Cement Technique in Total Hip Replacement", J. Bone Joint Surg., Vol. 65-A, 1983, pp. 1335-1338.

[51] Panjabi, M.M., Goel, V.K., Drinker, H., Wong, J., Kammire G., Walter, S.D., "Effect of Pressurization on Methylmethacrylate Bone Interdigitation: an *in vitro* Study of Canine Femora", J. Biomechanics, Vol. 16, 1983, pp. 473-480.

[52] Radin, E.L., Rubin, C.T., Thrasher, E.L., et al., "Changes in the Bone cement Interface After Total Hip Replacement: an *in vivo* Animal Study", J. Bone Joint Surg., Vol. 64-A, 1982, pp. 1188-1200.

[53] Reckling, F.W., Asher, M.A., Dillow, W.L., "A Longitudnal Study of the Radiolucent Line at the Bone-Cement Interface Following Total Joint Replacement Procedures", J. Bone Joint Surg., Vol. 59-A, 1977, pp. 355-358.

[54] Rhinelander, M.A., Nelson, C.L., Stewart, R.D., Stewart, C.L., "Experimental Reaming of the Proximal Femur and Acrylic Cement Implantation", Clinical Orthopaedics, Vol. 141, 1979, pp. 74-89.

[55] Rimnac, C.M., Wright, T.M., "The Effect of Centrifugation on the Fracture Properties of Poly(methylmethacrylate) Bone Cement", Trans. 31st O.R.S., Vol. 10, 1985, pg. 326.

[56] Rimnac, C.M., Wright, T.M., McGill, D.L., "The Effect of Centrifugation on the Fracture Properties of Acrylic Bone Cement", J. Bone Joint Surg., Vol. 68-A, 1986, pp. 281-287.

[57] Roark, R.J., Young, W.C., "Formulas for Stress and Strain", McGraw Hill, N.Y., 1975, pg. 600.

[58] Robinson, R.P., Wright, T.M., Burstein, A.H., "Mechanical Properties of Polymethylmethacrylate Bone Cements", J. Biomed. Mat. Res., Vol. 15, 1981, pp. 203-208.

[59] Ryd, L., "Micromotion in Knee Arthroplasty: A Roentgen Stereophotogrammetric Analysis of Four Concepts of Prosthetic Fixation", Ph.D. dissertation, University Hospital, Lund, Sweden, 1985.

[60] Salvati, E.A., Im, V.C., Wilson, P.D., "Radiology of Total Hip Replacements", Clinical Orthopaedics, Vol. 121, 1976, pp. 74-82.

[61] Shaw, D.W., "Finite Element Determination of K_I for a Completely Interdigitated Bimaterial Interface Crack", M.S. dissertation, Northwestern University, Evanston IL, June 1982.

[62] Sih, G.C., Berman, A.T., "Fracture Toughness Concept Applied to Methyl-methacrylate", J. Biomed. Mat. Res., Vol. 14, 1980, pp.311-324.

[63] Slooff, T.J.J.H., "The Influence of Acrylic Cement: An Experimental Study", Acta Orthop. Scand., Vol. 42, 1971, pp. 465-481.

[64] Stark, C.F., "Fracture and Fatigue Characteristics of Bone Cements", J. Biomed. Mat. Res., Vol. 13, 1979, pp. 339-342.

[65] Steege, J.W., Polizos, T., Lewis, J.L., Wixson, R.L., "Failure Mechanisms in PMMA Around Loaded Tibial Components", Trans. 32nd O.R.S., Vol. 11, 1986, pg. 355.

[66] Tapadiya, D., Walker, R.H., Schurman, D.G., "Prediction of Outcome of Total Hip Arthroplasty Based on Initial Postoperative Radiographic Analysis", Clinical Orthopaedics, Vol. 186, 1984, pp. 5-15.

[67] Tibrewal, S.B., Grant, K.A., Goodfellow, J.W., "The Radiolucent Line Beneath the Tibial Components of the Oxford Meniscal Knee", J. Bone Joint Surg., Vol. 66-B, 1984, pp. 523-529.

[68] Walker, P.S., Soudry, M., Ewald, F.C., McVickar, H., "Control of Cement Penetration in Total Knee Arthroplasty", Clinical Orthopaedics, Vol. 185, 1984, pp. 155-164.

[69] Willert, H-G., Ludwig, J., Semlitsch, M., "Reaction of Bone to Methacrylate After Hip Arthroplasty: a Long Term Gross, Light Microscope and Scanning Electron Microscope Study", J. Bone Joint Surg., Vol. 56-A, 1974, pp. 1368-1382.

[70] Williams, J.L., Lewis, J.L., "Properties and an Anisotropic Model of Cancellous Bone From the Proximal Tibial Epiphysis", J. Biomech. Eng., Vol. 104, 1982, pp. 50-56.

[71] Wright, T.M., Hayes, W.C., "Fracture Mechanics Parameters for Compact Bone-Effects of Density and Specimen Thickness", J. Biomechanics, Vol. 10, 1977, pp. 419-430.

[72] Wright, T.M., Burstein, A.H., Robinson, R.P.,"Fatigue Crack Propagation in Polymethylmethacrylate", Trans. 28th O.R.S., Vol. 7, 1982, pg. 182.

[73] Zand, M.S., Lewis, J.L., Santare, M.H., Steege, J.W., Wixson, R.L., "Bone Cement Pressure Distribution During Insertion of Posted Tibial Components", submitted to Journal of Orthopaedic Research.

[74] The Arthritis Foundation, Atlanta, GA, 1981.

[75] The Health Interview Survey, 1976, National Center for Health Statistics, HEW. reviewed in: Public Policy and Chronic Disease. A Forum Sponsored by the National Arthritis Advisory Board,U.S. Dept. Health, Education, and Welfare, Public Health Service, National Institute of Health, NIH Pub. 79-1896, 1979.

[76] Personal Communication; R.L.Wixson M.D.

[77] Bathe, K., Wilson, E.L., Peterson, F.E., "SAP IV: A Structual Analysis Program for Static and Dynamic Response of Linear Systems", University of California, Berkeley, California, 1974.

APPENDIX A: Procedure for Calculating ΔK

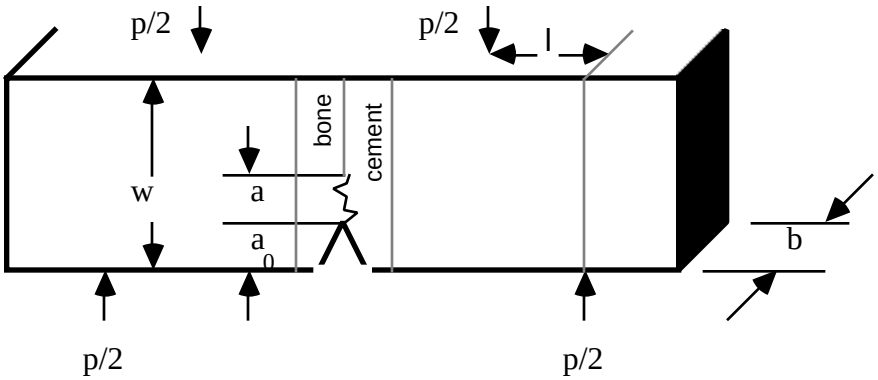

From Shaw [61] and Clech [13] it is shown that: $K/\sigma \Rightarrow f\{a/w\}$

The findings of Clech were used, who obtained the following equations by curve fitting his finite element results (letting $c = a + a_0$; $\Delta K/\sigma$ unit is $[in^{1/2}]$):

$$\frac{\Delta K}{\sigma} = \left(\frac{c}{w}\right)^{1/2} \{3.6323 - 8.2202 \left(\frac{c}{w}\right) + 4.9910 \left(\frac{c}{w}\right)^2 + 15.0881 \left(\frac{c}{w}\right)^3 - 2.0149 \left(\frac{c}{w}\right)^4\}$$

if the interface is considered to have no cohesive zone, and

$$\frac{\Delta K}{\sigma} = \left(\frac{c}{w}\right)^{1/2} \{3.8432 - 9.7472 \left(\frac{c}{w}\right) + 6.6601 \left(\frac{c}{w}\right)^2 + 17.1033 \left(\frac{c}{w}\right)^3 - 8.6988 \left(\frac{c}{w}\right)^4\}$$

if the interface is considered to have a cohesive zone.
The stress (σ) was obtained from beam theory:

$$\Delta\sigma = \frac{Mc}{I} = \frac{\frac{p}{2}\,l\,\frac{w}{2}}{\frac{1}{12}\,b\,w^3}$$

where $l = 0.020$ meters, $w = 0.025$ meters, and $b = 0.015$ meters.

Thus, if the finite element results are combined with the beam theory and p is in pounds:

$$\sigma = 28{,}467 \times p \quad \text{and}$$

$$\Delta K\,[Pam^{1/2}] = (\Delta K/\sigma) \times \Delta\sigma \times \left(0.1594\ \frac{m^{1/2}}{in^{1/2}}\right)$$

APPENDIX B: Plate Flexure of the Designed Device

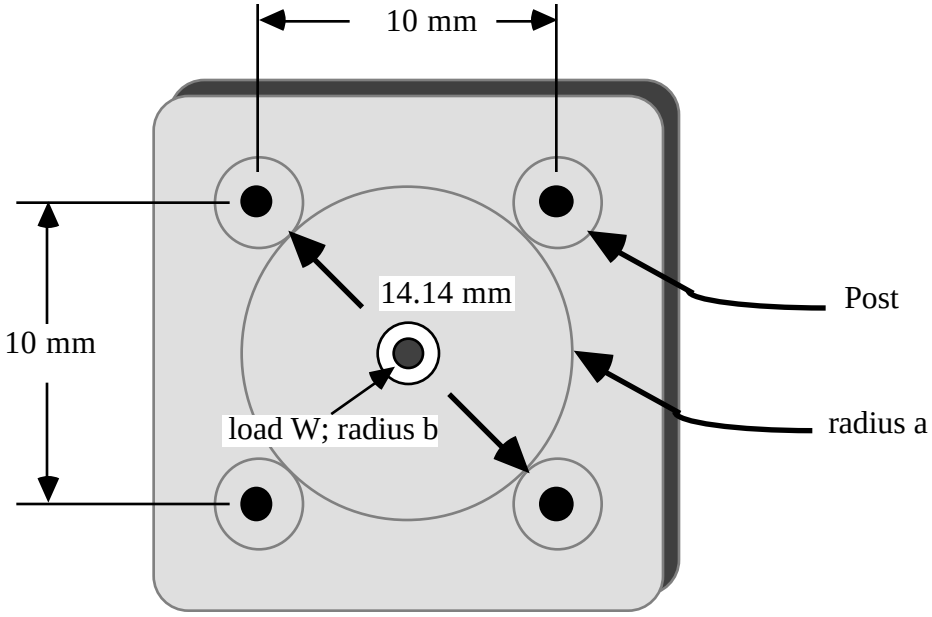

Consider the device to be fixed at each of the four posts. The situation may then be approximated as a circular plate rigidly fixed at its edge. The elementary equations governing this situation are:

$$y_{max} = \frac{-W a^2}{16 \pi D}$$

$$M_{r\,max} = \frac{W (1 + \upsilon)}{4 \pi} \ln \frac{a}{b}$$

$$\sigma_{r\,max} = \frac{6 M_{r\,max}}{t^2}$$

where: $D = E t^3 / 12 (1 - \upsilon^2)$

W = load

y = deflection

t = plate thickness

E = Young's modulus

υ = Poisson's ratio

M_r = radial moment

σ_r = radial stress

Assuming a near point load where W= 2000 Newtons (3 x body weight) and b = 0.5 t and using the material values reported in Table IV for titanium:

t [m]	y_{max} [μm]	$\sigma_{r\,max}$ [MPa]
0.001	132	2181
0.002	17	545

Thus, from this worst case analysis of a severe load situation, the thickness of the device should at least be 2 mm to avoid exceeding the yield stress of the metal and to reduce motion of the implant relative to the interface.

APPENDIX C: Post Fillet Calculation of the Designed Device

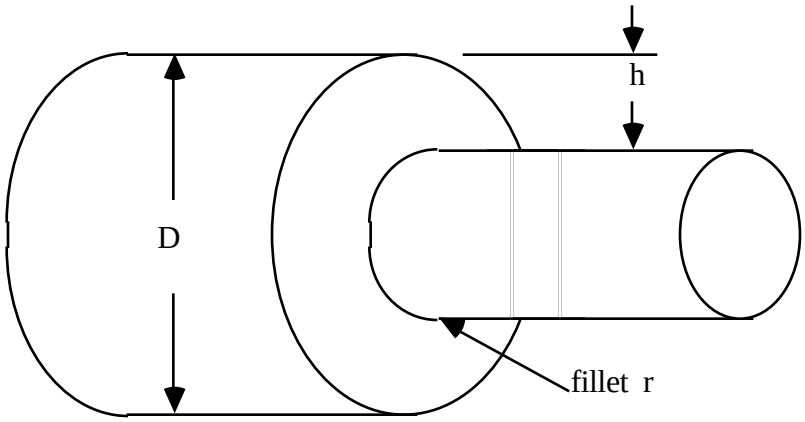

If it is assumed that a post and the surrounding plate may be modeled as a solid cylinder on a circular plate as shown above, it is found from reference [57]:

$$k = K_1 + K_{2\,x}\,(2h/D) + K_{3\,x}\,(2h/D)^2 + K_{4\,x}\,(2h/D)^3$$

if $2.0 < h/r < 20.0$ and where for:

$D = 14.14$ mm and $h = 5.57$ mm (so equations are valid for $0.28 < r < 2.8$ mm)

axial tension:
$K_1 = 1.225 + 0.831 \text{ x } (h/r)^{1/2} - 0.010 \text{ x } h/r$
$K_2 = -1.831 - 0.318 \text{ x } (h/r)^{1/2} - 0.049 \text{ x } h/r$
$K_3 = 2.236 - 0.522 \text{ x } (h/r)^{1/2} + 0.176 \text{ x } h/r$
$K_4 = -0.630 + 0.009 \text{ x } (h/r)^{1/2} - 0.117 \text{ x } h/r$

elastic bending:
$K_1 = 1.225 + 0.831 \text{ x } (h/r)^{1/2} - 0.010 \text{ x } h/r$
$K_2 = -3.790 + 0.958 \text{ x } (h/r)^{1/2} - 0.257 \text{ x } h/r$
$K_3 = 7.374 - 4.834 \text{ x } (h/r)^{1/2} + 0.862 \text{ x } h/r$
$K_4 = -3.809 + 3.046 \text{ x } (h/r)^{1/2} - 0.595 \text{ x } h/r$

elastic torsion:
$K_1 = 0.953 + 0.680 \text{ x } (h/r)^{1/2} - 0.053 \text{ x } h/r$
$K_2 = -0.493 - 1.820 \text{ x } (h/r)^{1/2} + 0.517 \text{ x } h/r$
$K_3 = 1.621 + 0.908 \text{ x } (h/r)^{1/2} - 0.529 \text{ x } h/r$
$K_4 = -1.081 + 0.232 \text{ x } (h/r)^{1/2} + 0.065 \text{ x } h/r$

It was found that for elastic bending and $r = 0.28$ mm that $k = 2.0$.

For design, k should be less than $\dfrac{\sigma_{\text{yield of metal}}}{\sigma_{\text{max at fillet}}}$

If the yield strength of titanium (from Table IV) is 800 MPa, then for $r = 0.28$ mm:

$\sigma_{\text{max at fillet}}$ must be kept less than 400 MPa.

This is an extremely high stress, thus it appears that the fillet radius may be very small indeed and this is desirable in order to provide a flush fit between device and bone.

TABLE Ia: Previous Studies on the Fracture of Compact Bone

Investigation	Method	Bone Origin	Orientation of fracture	G_c [$Jm^{-2} \times 10^3$]	K_c [$MNm^{-3/2}$]
Margel & Robertson [1973]	3 point bending	Bovine femur	longitudinal	-	6.56
Melvin & Evans [1973]	Single-edge notched	Bovine femur	Transverse longitudinal	1.39 - 3.14 - 5.53	2.56 3.21 5.58
Bonfield & Datta [1974]	Center notch (shock tube)	Bovine	Transverse tibia	4	0.23
Bonfield & Datta [1976]	Single-edge notched	Bovine tibia	longitudinal	0.78 - 1.12	2.2 - 4.6
Wright & Hayes [1977]	Compact tension	Bovine femur	Transverse	0.82	3.5
Bonfield, et al. [1978]	Compact tension	Bovine femur	Transverse	0.92 - 2.78	2.4 - 5.2
Behiri & Bonfield [1980]	Compact tension	Bovine tibia	Transverse	1.73 - 2.80	4.5 - 5.4
Behiri & Bonfield [1982]	Compact tension	Bovine tibia	Transverse	-	3.3 - 5.7
Behiri & Bonfield [1984]	Compact tension	Bovine tibia	longitudinal	1.02	4.0
Moyle & Bowden [1984]	3 point bend triangle xsect	Canine	longitudinal Human	9.0 ± 3.3 7.8 ± 2.1	- -

[In part compiled from Behiri & Bonfield, 1984]

TABLE Ib: Previous Studies on the Fracture of PMMA

Investigation	Method	PMMA	Preparation	K_c [$MNm^{-3/2}$]
Beaumont & Young [1975]	Double torsion	Simplex	Prepared in air	1.8 ± 0.1
		Simplex	Prepared in water	2.1 ± 0.1
Stark [1979]	Cantilever bending	Simplex		1.5 ± 0.2
		Zimmer		1.3 ± 0.1
Sih & Bermann [1980]	Compact tension	Simplex	No pressure, room temp.	1.56
		Simplex	Pressure, room temp.	1.58
		Simplex	No pressure, body temp.	1.20
		Simplex	Pressure, body temp.	1.55
Robinson, Wright, Burstein [1981]	3 point bending	Zimmer		1.4 ± 0.1
		Simplex		1.5 ± 0.1
		Zimmer	Carbon impregnated	1.9 ± 0.1
		Zimmer,LVC		1.2 ± 0.1
		Zimmer,LVC	Carbon impregnated	1.6 ± 0.1
Rimnac & Wright [1985]	Compact tension	Zimmer	Hand mixed	1.2 ± 0.3
		Palacos R		2.0 ± 0.2
		Zimmer	Centrifuged	1.2 ± 0.1
		Palacos R		2.0 ± 0.2

Previous Studies on the Fatigue of PMMA

Investigation	Method	PMMA	Preparation	Initial Stress [MPa]	Fail. Cycles [log(N)]
Frietag [1976]		Zimmer	Hand mixed	8.6	5.2 ± 4.5
		Simplex P	Hand mixed	8.6	5.8 ± 5.2
Stark [1979]	Waisted	Zimmer	Hand mixed, 5 psi	6.9	6.0
		Zimmer	Hand mixed, 25 psi	6.9	6.1
		Zimmer	Hand mixed, 50 psi	6.9	6.0
		Simplex	Hand mixed, 5 psi	6.9	6.4
		Simplex	Hand mixed, 25 psi	6.9	6.3
		Simplex	Hand mixed, 50 psi	6.9	6.3
Gates, et al. [1984]	Waisted	Simplex	Hand mixed	14.9	3.4 ± 0.6
		Zimmer,LVC	Centrifuged	15.4	3.1 ± 0.4
Krause & Mathis [1984]	Waisted	Simplex	Hand mixed	47.9	2.8 ± 2.6
		Zimmer	Hand mixed	40.6	3.1 ± 2.6
		Zimmer,LVC	Hand mixed	32.0	3.7 ± 3.4
Davies, et al. [1985]	Waisted	Simplex	Hand mixed	15.0	4.2 ± 3.4
		Simplex	Centrifuged	15.0	4.5 ± 4.2
		Zimmer	Hand mixed	15.0	2.9 ± 2.7
		Zimmer	Centrifuged	15.0	3.9 ± 3.7
		Zimmer,LVC	Hand mixed	15.0	3.4 ± 3.1
		Zimmer,LVC	Centrifuged	15.0	3.9 ± 3.7

TABLE II: Data

Test Number	Bone Type	Bone Strength [MPa]	Grade	Penetration Depth [mm]	Grade	Application Pressure [KPa]	Applied Load [N]	Initial Crack length [mm]	Initial Crack opening [μm]	Failure Cycles [log(N)]
N1a1	tibia	5.34	2	0.10	1	197	178	-	-	-
N1a2	tibia	5.34	2	4.08	3	197	489	4.9	-	2.50
N3b	tibia	4.82	2	1.32	1	049	222	-	-	-
N3d	tibia	4.62	2	3.13	2	122	267	5.2	-	2.84
N4a	femur	5.21	2	3.67	2	197	489	5.5	-	3.42
N4b	femur	2.49	1	1.70	1	036	133	-	-	-
N5b	femur	5.69	2	1.75	1	121	356	-	-	-
N5c	femur	2.24	1	2.77	1	121	133	-	-	-
N5d	femur	4.75	2	4.61	3	197	267	-	-	-
N6b	femur	2.10	1	2.78	1	076	178	-	-	-
S1a	femur	5.06	2	2.29	1	138	178	4.5	50	5.44
S1b	femur	8.47	3	2.48	1	138	178	5.3	72	4.16
S1c	femur	3.58	2	3.89	2	138	178	5.0	48	5.71
S3b	femur	8.38	3	3.57	2	138	178	4.4	36	≥ 5.74
S6a	femur	3.79	2	4.57	3	138	178	5.0	-	≥ 5.49
S6b	femur	7.76	3	5.30	3	138	356	5.4	120	3.30
S6c	femur	3.79	2	5.94	3	138	178	4.3	-	≥ 5.20
S10a	femur	5.25	2	3.54	2	138	178	5.2	37	5.73
S10c	femur	8.09	3	4.56	3	138	267	4.9	61	5.35
S13a1	femur	9.64	3	0.10	1	-	178	-	-	0.00
S13a2	femur	9.64	3	3.50	2	-	311	4.1	45	5.75
S13b	femur	3.77	2	6.93	3	138	178	5.2	52	5.58
Z3a	tibia	5.04	2	1.45	1	035	035	4.0	50	4.92
Z5a	tibia	3.00	2	1.40	1	035	067	4.5	42	4.17
Z9a	tibia	1.15	1	1.12	1	035	089	4.4	107	3.00
Z11a	tibia	1.97	1	0.51	1	035	051	4.8	52	1.48
mean		4.81		2.96		116	192	4.8	59	≥ 5.27
standard dev.		2.33		1.77		60	127	0.5	26	5.33
•A5d*	femur	3.99	2	3.73	2	-	178	5.2	32	≥ 5.70
¢A6d*	femur	8.42	3	2.80	1	-	311	5.0	42	≥ 4.85
•AZ5a*	tibia	3.00	2	5.60	2	-	267	4.4	32	≥ 5.30
mean*		5.14		4.04			252	4.9	35	≥ 5.41
standard dev.*		2.89		1.43			68	0.4	6	5.34

• - test stopped; ¢ - support interface fracture; * - Crack arrestor trials

TABLE III: Cohesive Zone Data
[used by Clech]

Specimen Number	Primary Crack Length [mm]	Secondary Crack Length [mm]	Cohesive Zone Size [mm]
S1a	8.0	6.0	2.0
S1b	8.0	5.3	2.7
	12.5	8.5	4.0
	16.0	10.0	6.0
	16.8	11.5	5.3
	17.0	13.4	3.6
S3b	13.5	9.0	4.5
S6a	11.1	5.0	6.1
S6b	10.4	6.0	4.4
S13b	12.2	8.0	4.2
	13.0	8.5	4.5
	15.0	10.0	5.0
	16.0	12.0	4.0
	16.5	12.3	4.2

The mean cohesive zone length of this study (λ) was:
4.15 ± 1.77 mm (n=284 measurements)

TABLE IV: Biomedical Material Values

Material	Young's Modulus [Pa]	Yield Strength [Pa]	Poisson's Ratio
CoCr-Mo Alloy	2.1×10^{11}	4.7×10^{8}	
Steel, cast 316L	2.0×10^{11}	2.4×10^{8}	
Titanium, Ti6Al4V	1.1×10^{11}	8.0×10^{8}	0.33
Cortical Bone	1.5×10^{10}	1.5×10^{8}	0.28
PMMA	2.1×10^{9}	3.0×10^{7}	0.40
UHMW Polyethylene	1.0×10^{9}	2.0×10^{7}	
Cancellous Bone	3.3×10^{8}	$1\text{-}10 \times 10^{6}$	

Figure 1.1: Radiograph of an *in vivo* Kinematic™ posted tibial component exhibiting a radiolucent line.

Figure 1.2: Scanning Electron Micrograph (x 280) of cement cracks originating from cement beads exposed to a compression load (1334 N) for 390,000 cycles during an *in vitro* implant simulation test performed by Steege et al. [65].

Figure 1.3: Scanning Electron Micrograph (x 78) of cement cracks originating from cement voids (right) and the metal/cement interface (left) exposed to a tensile load (667 N) for 200,000 cycles during an *in vitro* implant simulation test performed by Steege et al. [65].

Figure 1.4: Light microphotograph (x 100) of cement cracks originating from cement voids after being exposed to a compression load (1334 N) for 390,000 cycles during an *in vitro* implant simulation test performed by Steege et al. [65].

Figure 1.5: Radiograph of an *in vivo* Kinematic™ posted tibial component with an initial flaw at the bone/cement interface (upper right corner).

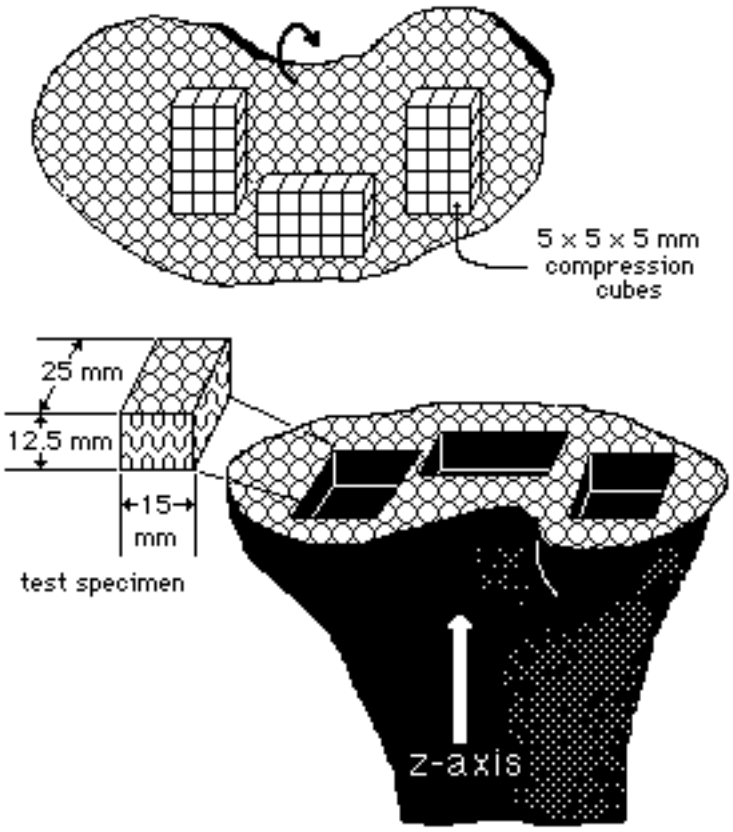

Figure 2.1: Schematic showing typical origin of bone specimens from a cadaver tibia.

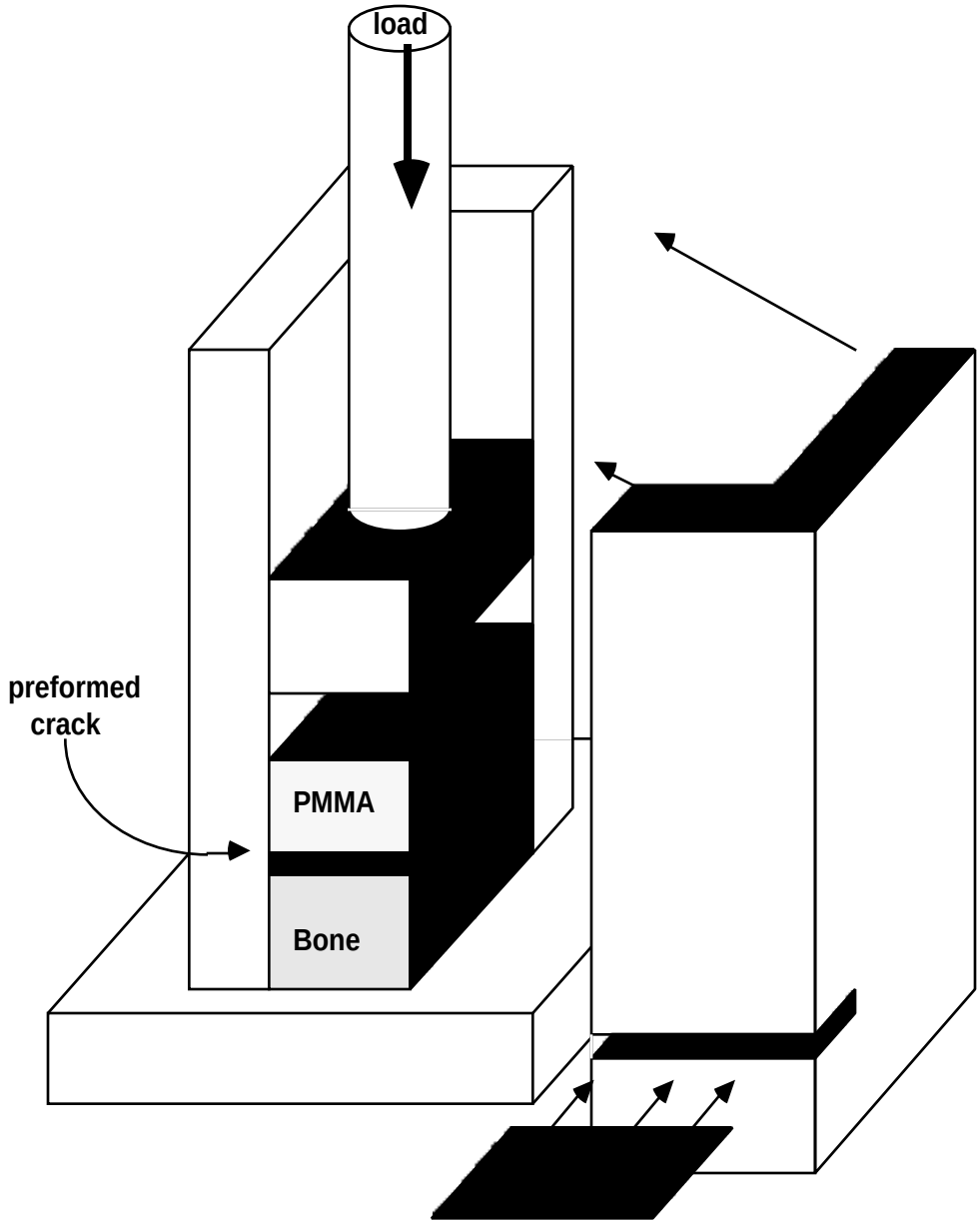

Figure 2.2: Schematic of the jig used to form the bone cement interface of the specimens.

Figure 2.3: Radiograph (x 2) of specimen S13b showing the degree of cement (upper) penetration into the cancellous bone cube (lower). Note the 5 mm initial crack on the right.

Figure 2.4: Radiograph of specimen N5b after fracture showing the degree of cement (upper) penetration into the cancellous bone cube (lower).

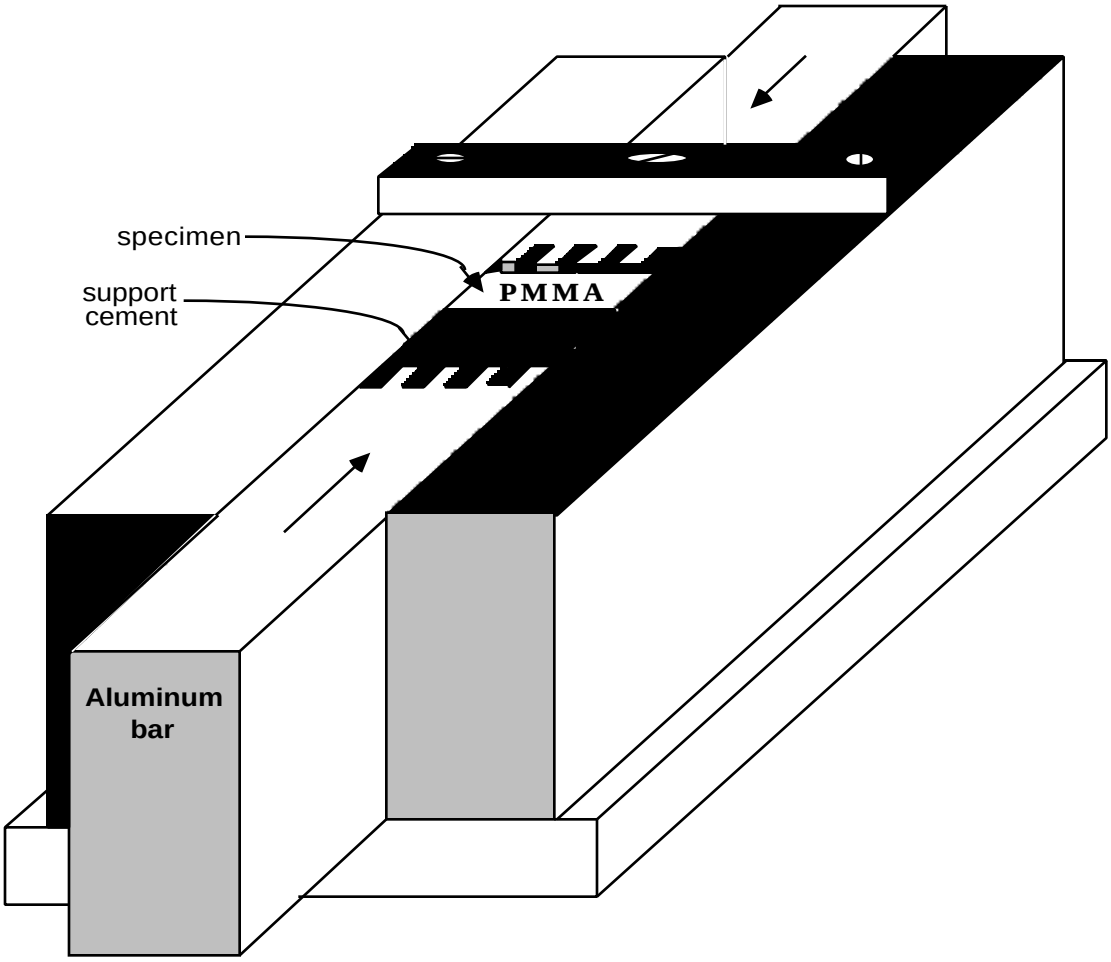

Figure 2.5: Jig used to assemble the bone-PMMA specimen into its final testable beam configuration. Low viscosity cement was used to bind the specimen to each of the aluminum bars to form the beam.

Figure 2.6: Photograph of the final four-point bent beam test configuration. Note the clip gage attachment (MTS) across the crack mouth.

Figure 2.7: Schematic of the final four-point bent beam test configuration pictured in Figure 2.6.

Figure 3.1: Specimen S10a in bending under 67 Newtons of load applied from above after 533,000 cycles at 178 Newtons of load. Note the large secondary crack extending to approximately the 13.1 cm mark of the small scale.

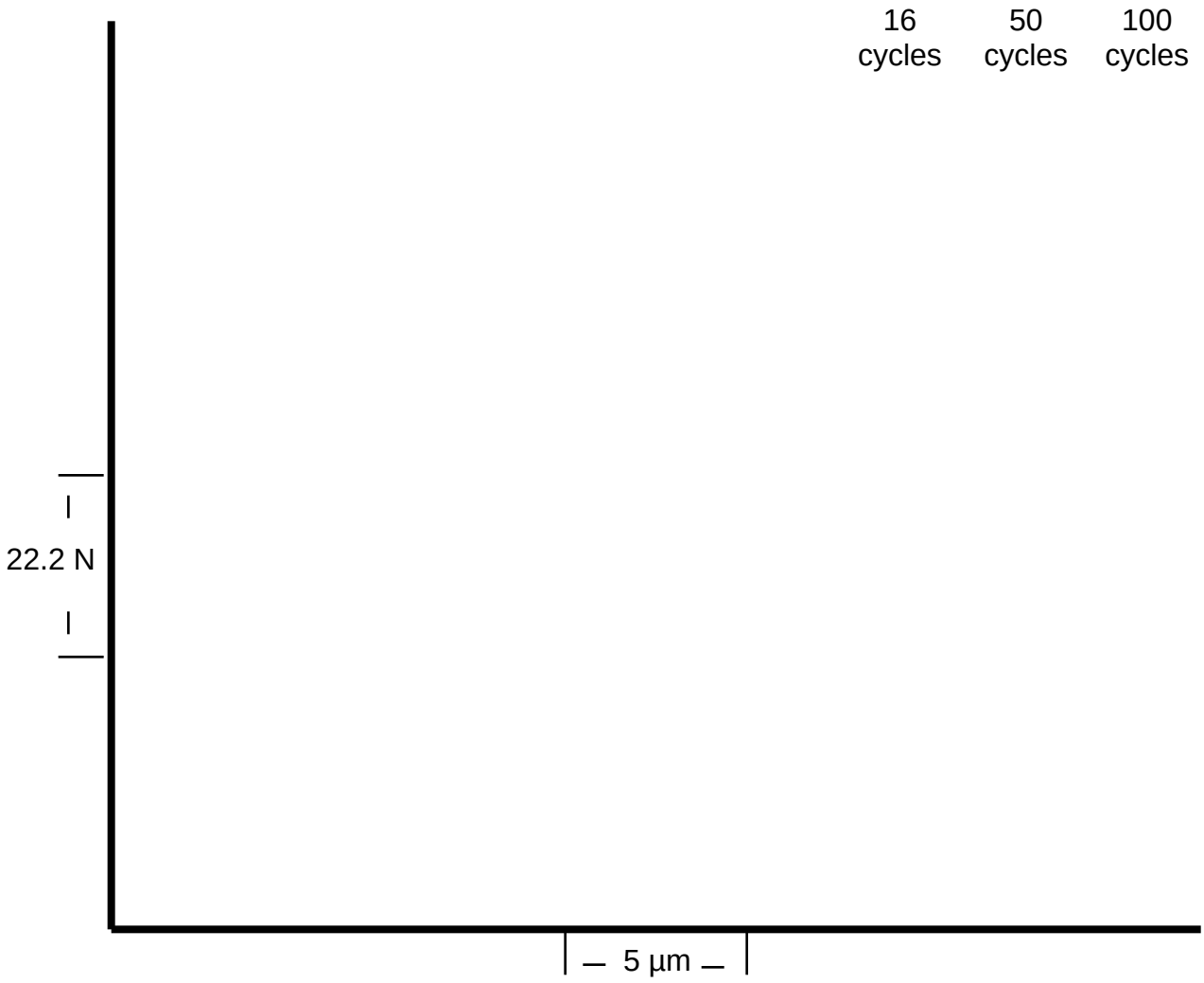

Figure 3.2: Typical load vs crack mouth opening plot (specimen Z9a) obtained during cyclic loading. Note permanent crack opening present as the load returns to zero and the number of cycles increase.

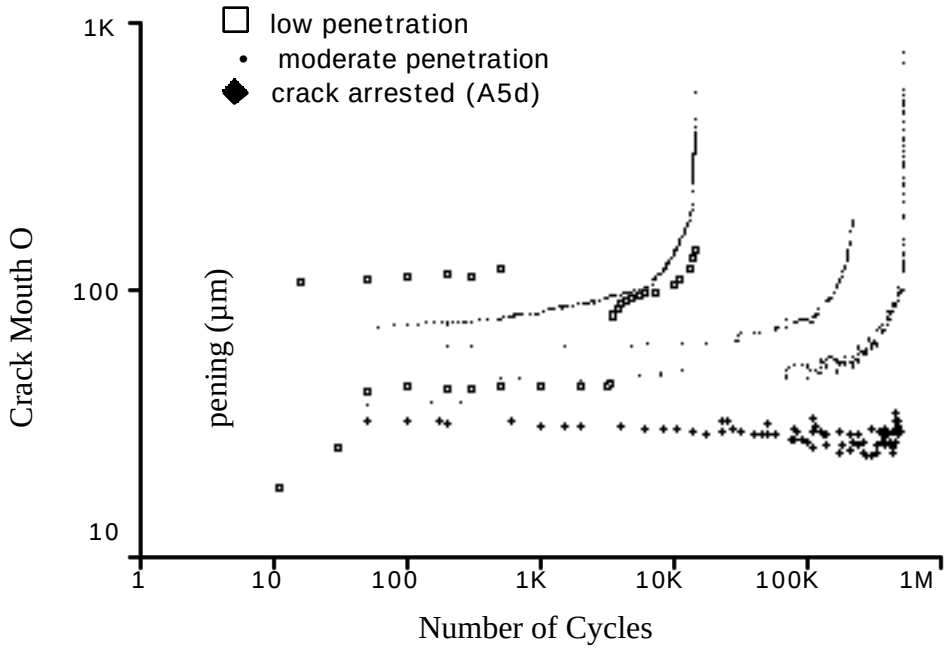

Figure 3.3: Log:Log plot of Crack opening vs number of cycles for several specimens. Note the relative low opening for the crack arrested case.

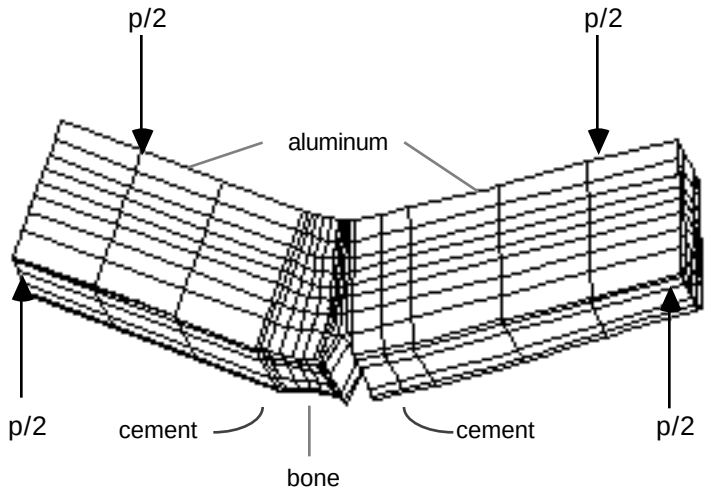

Figure 3.4: The finite element mesh of the beam showing the deformed shape (x 100) for a 178 Newton load (p) applied as shown. This particular model was for a specimen with a 5 mm initial crack.

Figure 3.5: PMMA surface (initial crack at left) of specimen S10a following final failure after 534,000 cycles under 178 Newtons of load. Note individual fractured cement spicules.

Figure 3.6: Scanning Electron Photomicrograph (x 15) of the fracture surface of specimen S10a pictured in Figure 3.2.

Figure 3.7: Scanning Electron Photomicrograph (x 15) of the fracture surface of specimen S13b after failure at 178 Newtons for 380,000 cycles.

Figure 3.8: Photograph of specimen S10a with no load applied after 533,000 cycles showing permanent crack opening (approximately 230 μm) on the bottom near the initial crack.

Figure 3.9: Plot showing all of the measured primary, secondary, and cohesive zone lengths (with corresponding regression lines) in millimeters vs the crack mouth opening in microns as measured by the extensometer gage.

Figure 3.10: A typical crack extension vs total cycles plot (specimen N3b).

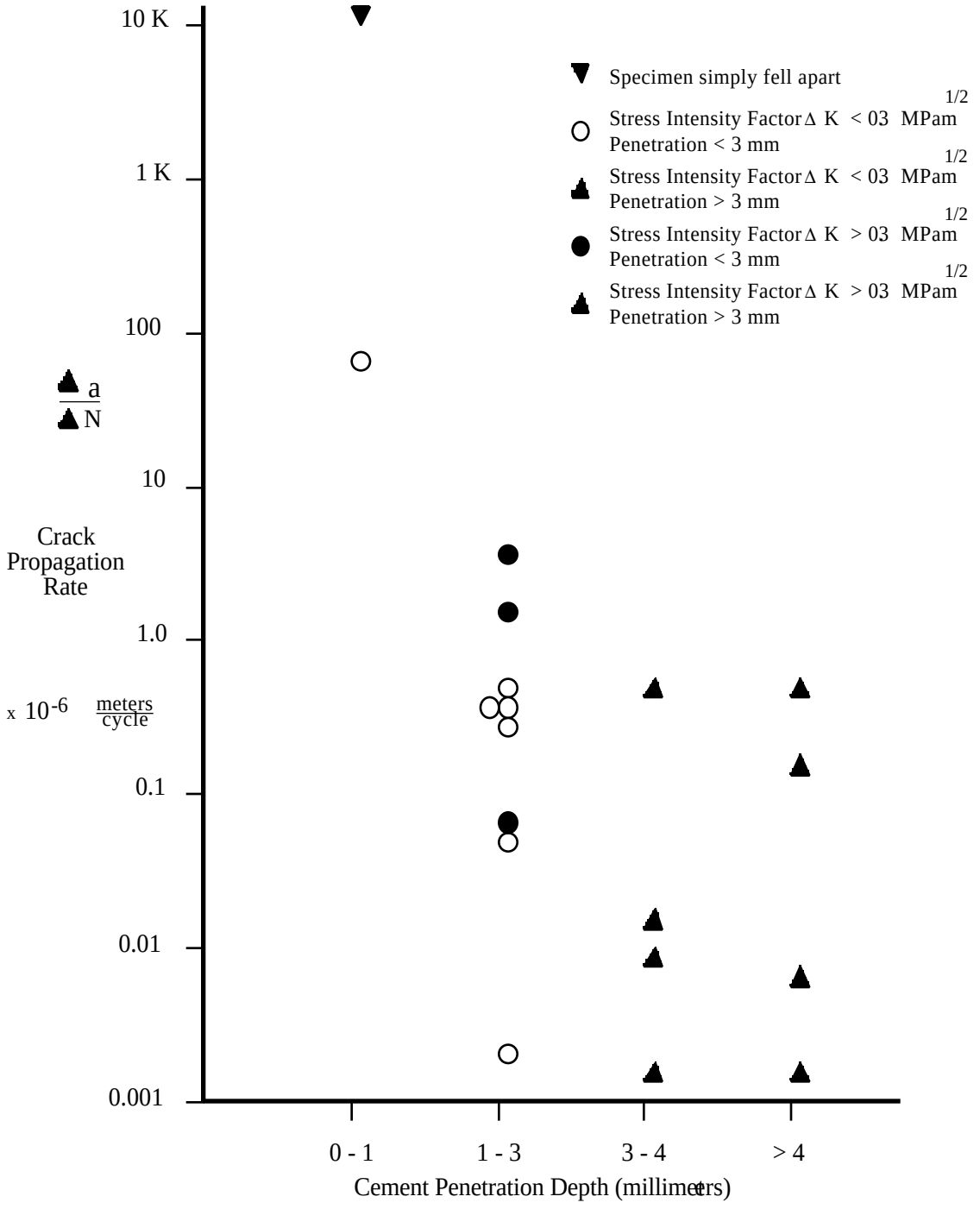

Figure 3.11: Plot of measured primary crack propagation rate vs cement penetration.

Figure 3.12: Plot of primary crack length vs ln{cycle} as a function of cement penetration depth and stress environment for several specimens used in the study. Note the specimens marked with a $*$ correspond to the posted specimens A5d (Δ) and A6d (**.**).

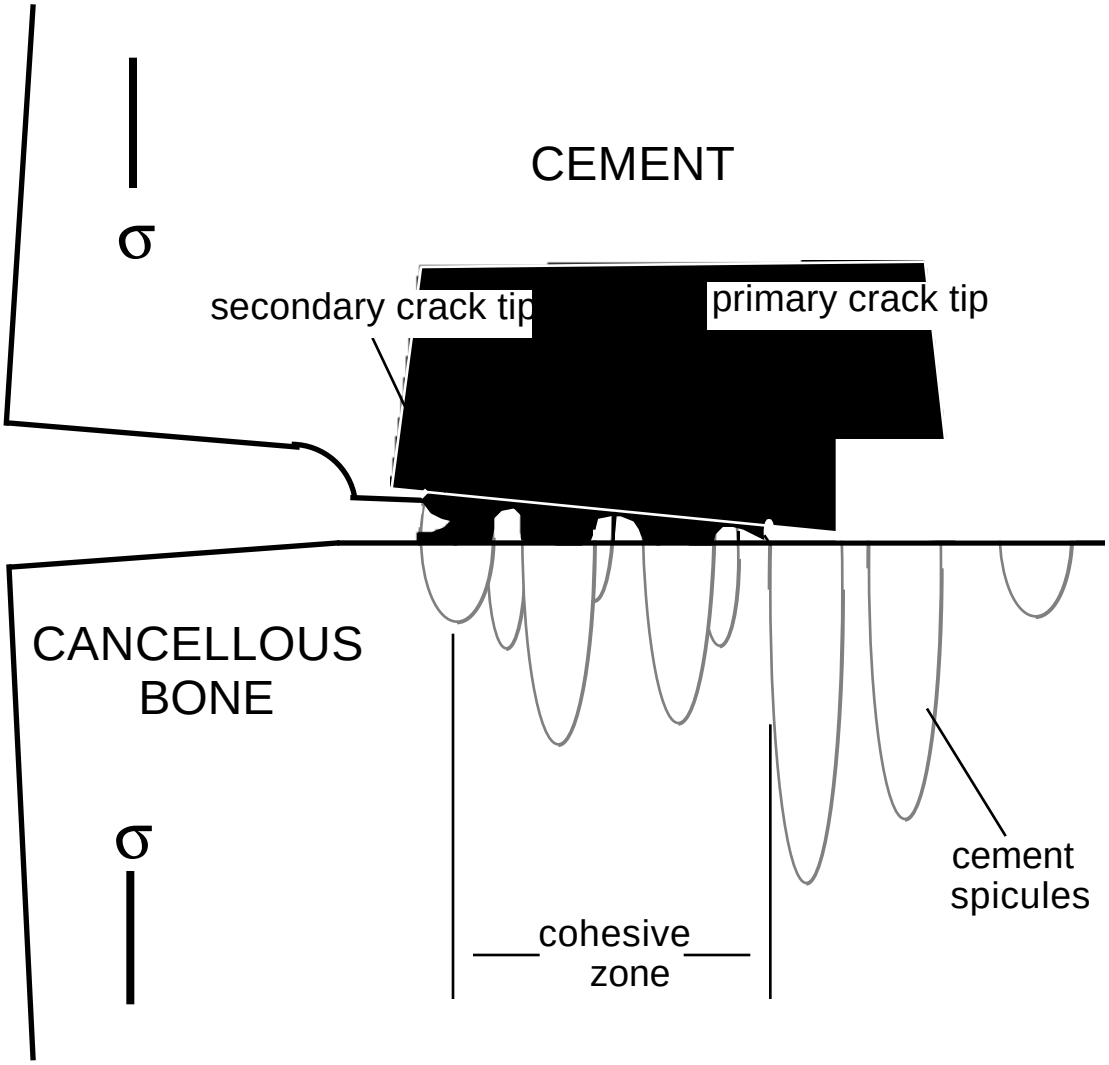

Figure 3.13: Schematic of the primary crack and cohesive zone as modeled by Clech.

Figure 3.14: Plot of measured crack propagation rate with computed regression lines {Eq. 3.6} for region(s) 2 vs the cyclic stress intensity factor at the crack tip as a function of cement penetration and bone strength values.

Figure 3.15: Plot of measured crack propagation rate with computed regression line {for Eq. 3.6} for region 1 {Eq. 3.9; dark points} and region(s) 2 {Eq. 3.6; light points} vs the cyclic stress intensity factor at the crack tip as a function of cement penetration and bone strength values.

Figure 3.16: Plot of the measured number of crack discontinuity occurrences ($Post_N$) with regression line {Eq. 3.7} vs the interface primary crack length.

Figure 3.17: Plot of the measured number of cycles per crack discontinuity (N_{post}) with regression lines {Eq. 3.8} vs the cyclic stress intensity factor at the crack tip as a function of cement penetration depth and bone strength values.

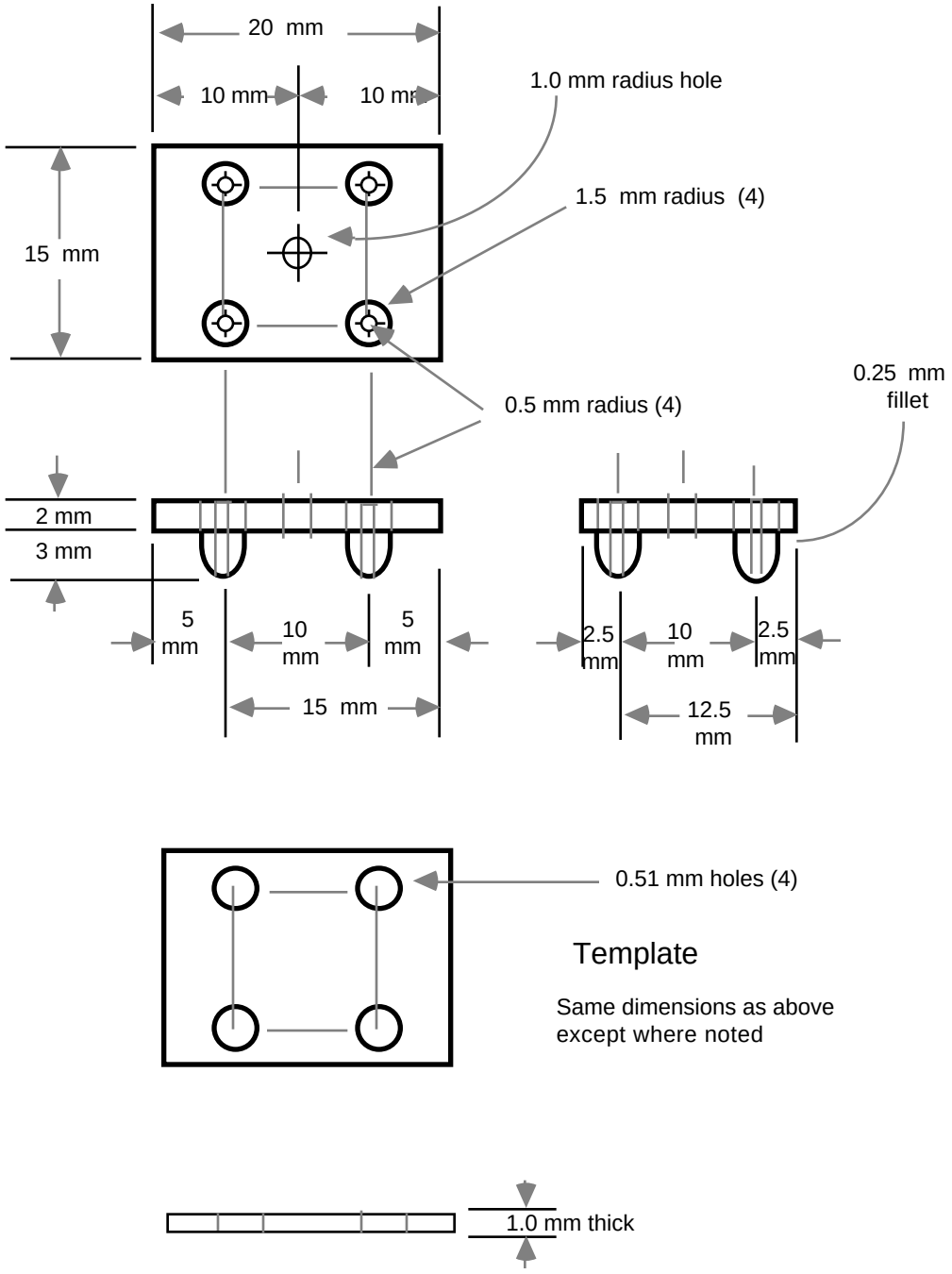

Figure 4.1: Schematic of designed 'crack arrestor' device.

Figure 4.2: Photograph of ‘crack arrestor’ device (right) with alignment template (left).

Figure 4.3: Close-up photograph of the underside of the ‘crack arrestor’ device.

Figure 4.4: Radiograph of specimen A5d (with ‘crack arrestor’ device) in its four-point bent beam configuration.

Figure 4.5: Photograph of specimen A5d after 500,000 cycles at 178 Newtons and then being linearly loaded to failure at 706 Newtons. Note failure through a ‘subinterface’ layer of bone.

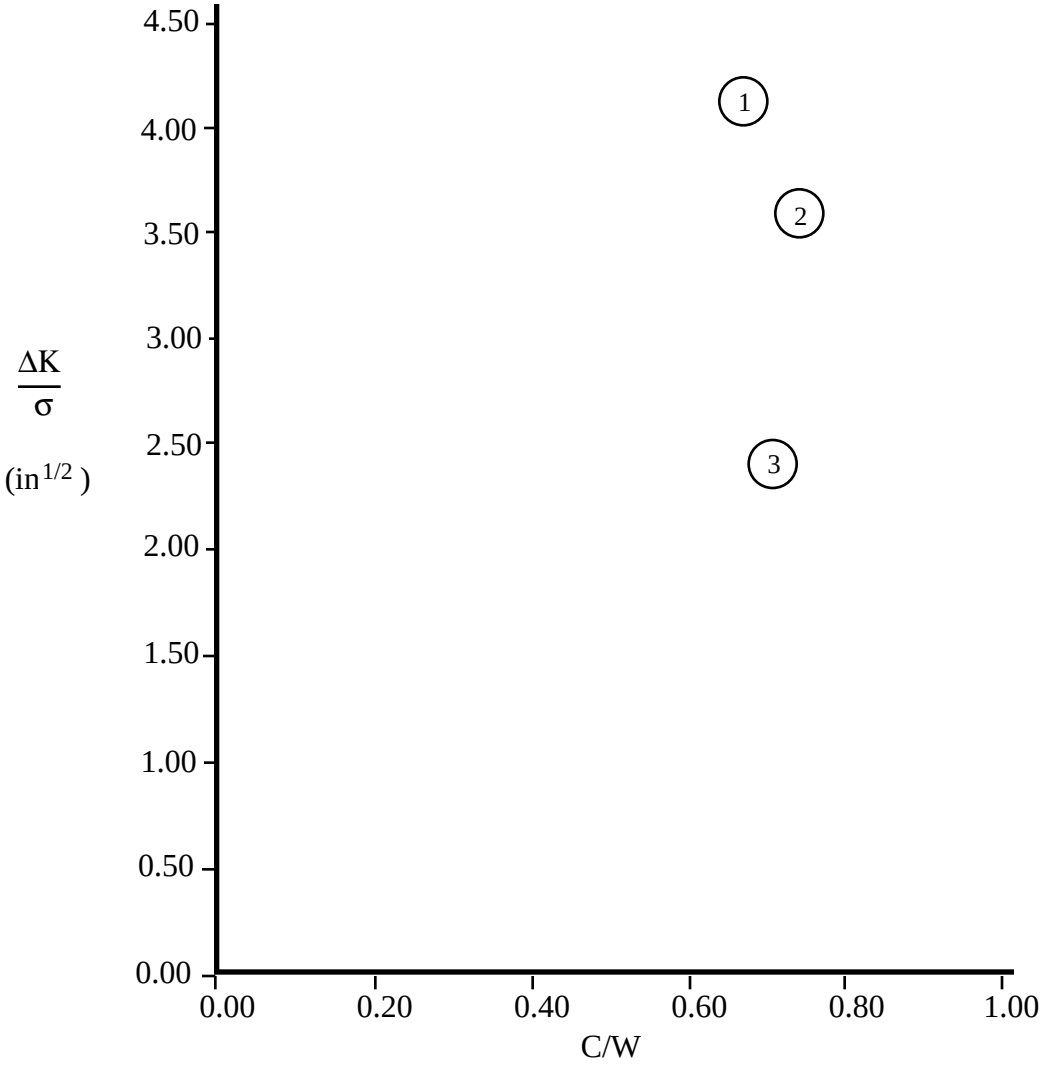

Figure A.1: Plot of Clech's [13] and Shaw's [61] results for a finite element model of the four-point bent beam configuration used in this study where (c/w) is the ratio of the primary crack length to the total specimen width (25 mm). 1) Clech, no cohesive zone modeled 2) Clech, cohesive zone modeled 3) Shaw